Heliyon 8 (2022) e10384

Contents lists available at ScienceDirect

Heliyon

journal homepage: www.cell.com/heliyon

Research article

Transplantation of IGF-1-induced BMSC-derived NPCs promotes tissue repair and motor recovery in a rat spinal cord injury model

Putri Nur Hidayah Al-Zikri [a,b,1], Tee Jong Huat [c,b,1,2], Amir Ali Khan [d,**], Azim Patar [b,f], Mohammed Faruque Reza [b,f], Fauziah Mohamad Idris [e], Jafri Malin Abdullah [b,f,*], Hasnan Jaafar [a]

[a] Department of Pathology, School of Medical Sciences, University Sains Malaysia, Kelantan, Malaysia
[b] Department of Neurosciences, School of Medical Sciences, University Sains Malaysia, Kelantan, Malaysia
[c] Department of Biological Sciences, National University of Singapore 117543, Singapore
[d] Department of Applied Biology, College of Sciences, University of Sharjah, Sharjah, P. O. Box 27272, United Arab Emirates
[e] Department of Medical Microbiology, School of Medical Sciences, University Sains Malaysia, Kelantan, Malaysia
[f] Brain Behaviour Cluster, School of Medical Sciences, University Sains Malaysia, Kelantan, Malaysia

GRAPHICAL ABSTRACT

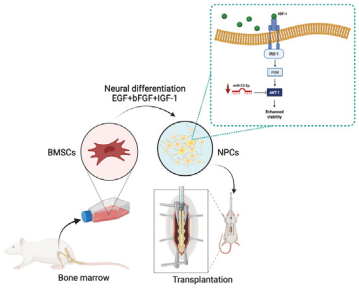

ARTICLE INFO

Keywords:
Mesenchymal stem cell
Growth factor
Neural differentiation
microRNA
Cell therapy
Spinal cord injury

ABSTRACT

Bone marrow-derived mesenchymal stem cells (BMSCs) have therapeutic potential for spinal cord injury (SCI). We have shown that insulin-like growth factor 1 (IGF-1) enhances the cellular proliferation and survivability of BMSCs-derived neural progenitor cells (NPCs) by downregulating miR-22-3p. However, the functional application of BMSCs-derived NPCs has not been investigated fully. In this study, we demonstrate that knockdown of endogenous miR-22-3p in BMSCs-derived NPCs upregulates *Akt1* expression, leading to enhanced cellular proliferation. RNASeq analysis reveals 3,513 differentially expressed genes in NPCs. The upregulated genes in NPCs enrich the gene ontology term associated with nervous system development. Terminally differentiated NPCs generate cells with neuronal-like morphology and phenotypes. Transplantation of NPCs in the SCI rat model results in better recovery in locomotor and sensory functions 4 weeks after transplantation. Altogether, the result of this study demonstrate that NPCs derived with IGF-1 supplementation could be differentiated into functional neural lineage cells and are optimal for stem cell therapy in SCI.

* Corresponding author.
** Corresponding author.
E-mail addresses: amkhan@sharjah.ac.ae (A.A. Khan), brainsciences@gmail.com (J.M. Abdullah).
[1] These authors contributed equally.
[2] Lead contact: Tee Jong Huat, PhD (teejonghuat@gmail.com).

https://doi.org/10.1016/j.heliyon.2022.e10384
Received 27 January 2022; Received in revised form 14 April 2022; Accepted 15 August 2022

1. Introduction

Traumatic spinal cord injury (SCI) is a common and devastating nervous system disorder that often results from accidents. The pathophysiology of SCI involves a primary injury that directly disrupts nerve cells and surrounding blood vessels. Undermanaged primary injury leads to secondary injury cascades, such as inflammation, vascular dysfunction, ischemia, edema, and excitotoxicity. These symptoms perturb communication between the brain and the body, resulting in the loss of voluntary movements and sensation below the damaged plane (Hosseini et al., 2018; Tran and Silver, 2015).

Because of the slow regenerative capability of the central nervous system (CNS) cells upon injury, the treatment of SCI remains a therapeutic challenge. Surgical re-stabilization of the vertebral column and rehabilitation are the current medical practices to prevent secondary complexities and to provide support to the patient (Sandean, 2020). Despite the overall advancement in medical and surgical care, which has improved the outcomes for SCI patients, no effective treatment is currently available for neurological deficits after SCI.

Stem cell-based therapies using embryonic stem cells, neural stem cells, or mesenchymal stem cells (MSCs) are emerging approaches for spinal cord repair. The use of stem cells to treat neurodegenerative diseases, such as SCI, has been extensively studied (Kim et al., 2016; Qu and Zhang, 2017; Duncan and Valenzuela, 2017). In fact, stem cell therapy offers a wide range of medical benefits against SCI, such as axon re-myelination, restoration of neuronal circuitry, reduced inflammation, and promotion of angiogenesis (Xiong et al., 2010). Among MSCs from different sources, bone marrow-derived MSCs (BMSCs) are promising alternatives for the treatment of neurodegenerative disorders because of their easy accessibility, expandability *in vitro*, unique immunogenic properties, and capability to differentiate into neural cell types (Tanna and Sachan, 2014; Ankrum et al., 2014; Alexanian et al., 2008; Mezey et al., 2003).

BMSCs are multipotent stem cells capable of differentiation into many cell types, such as chondrocytes, adipocytes, osteocytes, and neural lineage cells (Takeda and Xu, 2015; Bai et al., 2004). It has been reported that BMSC transplantation enhanced axonal regeneration and promoted functional recovery in spinal cord injury animal models (Lee et al., 2003). Recently, a study has shown that intrathecal transplantation of allogeneic BMSCs did not produce neurological deficits or immune rejection against donor cells in a canine model (Benavides et al., 2021). Similarly, studies have reported that both autologous and allogeneic BMSCs can be safely administered in SCI patients (Pan et al., 2019; Karamouzian et al., 2012; Vaquero et al., 2017; Satti et al., 2016). All these pieces of evidence suggest that BMSCs could be a potential therapy for irreversible damage to the CNS.

In our earlier study, we reported a protocol for the differentiation of BMSCs into neural progenitor-like cells (NPCs) by the supplementation of insulin-like growth factor 1 (IGF-1) into the culture media along with epidermal growth factor (EGF) and basic fibroblast growth factor (bFGF). The addition of IGF-1 generated better neurospheres than those produced using only a combination of EGF and bFGF in terms of cell survivability and proliferation (Huat et al., 2014). MicroRNA profiling of BMSC-derived NPCs delineated several key microRNAs associated with IGF-1 supplementation, with mir-22-3p being the most strikingly downregulated microRNA.

MiR-22-3p is a neuron-related microRNA expressed in the neurites (Fiumara et al., 2015). Overexpression of miR-22-3p induced cell senescence and decreased proliferation and migration of endothelial progenitor cells, whereas suppression of miR-22-3p showed reversed effects (Zheng and Xu, 2014). MiR-22-3p has also been reported to regulate the cell cycle during cerebellum development by targeting the *Max* and *Myc* genes (Berenguer et al., 2013). Despite vast information on miR-22-3p, how IGF-1 regulates miR-22-3p expression involved in the enhancement of BMSC differentiation toward NPCs remains unclear. The functional properties of BMSCs-derived NPCs also remain understudied. We hypothesize that NPCs derived under EGF, bFGF, and IGF-1 supplementation could better promote the recovery of the injured spinal cord in a rat model.

In this study, we first investigate the role of miR-22-3p in cellular proliferation and survivability of BMSC-derived NPCs via the loss-of-function approach. We also perform RNASeq of BMSCs-derived NPCs to elucidate the transcriptomic alterations during the differentiation of the BMSCs into a neural lineage. We validate the functional properties of BMSC-derived NPCs using both an electrophysiological approach and transplantation of NPCs into a rat SCI model. Overall, our experiment reveals that transplantation of NPCs derived under the influence of bFGF, EGF, and IGF-1 promotes better recovery of the injured spinal cord and improves sensory and motor functions in the rat SCI model.

2. Results

2.1. Primary Isolated BMSCs and Neural Induction

The characteristics of primary isolated BMSCs were determined using selected cell surface markers and the capability of BMSCs to differentiate into mesodermal lineage cells (Dominici et al., 2006). BMSCs exhibited fibroblast-like morphologies at 90% confluency *in vitro;* they expressed surface antigens CD90, CD44, fibronectin, vimentin and weakly expressed nestin (Figure 1A), whereas they were negative against the CD11b marker (Figure S1A). Moreover, BMSCs can differentiate into adipocytes, chondrocytes, and osteocytes under specific differentiation media. BMSC-derived adipocytes formed lipid droplets and were stained with oil red O staining. Dense chondrocytes were stained with alcian blue, whereas calcium deposits stained with alizarin red S were observed in the osteogenic differentiation (Figure S1B). Upon differentiation in the neural induction media, adherent BMSCs developed into floating neurosphere-like cells whose size increased with time (Figure 1B). Growth factor supplemented NPCs showed heterogeneous spherical shapes in the population of clonal neurospheres, whereas the neural basal only group appeared irregular in shape, with uneven surface morphology. Neurospheres derived with IGF-1 supplementation exhibited outstanding morphological features, and they had the largest colony size among the groups. Neurosphere-like cells from all groups expressed Sox2 and had low expression levels of fibronectin (Figure 1C). These data suggest that the BMSCs have differentiated into a neural lineage.

2.2. Involvement of MiR-22-3p in the cellular proliferation of BMSC-derived NPCs

The cell proliferation assay was used to evaluate the effects of growth factors on NPC proliferation. Both growth factor-treated groups showed significant differences ($p < 0.05$) compared with the control group throughout the experimental period (five time intervals: 24 h, 48 h, 72 h, 96 h, and 120 h) (Figure 1D). Multiple comparisons among groups demonstrated that those groups supplemented with growth factors had better proliferative activities than the neural basal only group. Notably, NPCs with IGF-1 supplementation showed the highest proliferation.

Our earlier microarray analysis reported the downregulation of miR-22-3p in NPCs derived under EGF + bFGF + IGF-1 supplementation (Huat et al., 2015b). Bioinformatic analysis revealed that *Akt1*, *Pten*, and *Tp53*, enriched in the negative regulation of apoptosis, GO:0043066, are potential targets of miR-22-3p. Therefore, the endogenous expression of miR-22-3p and the predicted targets were measured using quantitative real-time PCR (qPCR). Indeed, miR-22-3p expression in NPCs (EGF + bFGF + IGF-1) was significantly downregulated compared with both the control and NPCs (EGF + bFGF) (Figure 1E). Consistently, *Akt1*, *Pten*, and *Tp53* were consistently upregulated in growth factors treated groups compared with the control (Figure 1F). Notably, *Akt1* was significantly expressed in the presence of IGF-1. Thus, we postulated that the enhanced proliferation of NPCs in the presence of IGF-1 could be due to the suppression of miR-22-3p.

To further confirm the role of miR-22-3p, we performed a knockdown of endogenous miR-22-3p in BMSCs using the synthetic miR-22-3p inhibitor before neural induction. Co-transfected fluorescent-labelled miRNA was detected within the cytoplasm and nuclei of the BMSCs after 24 h of transfection (Figure S2A). More than 90% of the BMSCs were transfected and remained constant up to the third day *in vitro* (Figure S2B). The cells also remained viable throughout the experimental period (Figure S2C). Using the 24 h transfected BMSCs, we performed neural induction, as described earlier, and monitored the cells at 72 h. BMSCs transfected with scramble miRNA differentiated into larger neurospheres when supplemented with EGF + bFGF + IGF-1 compared with the condition without IGF-1. By contrast, NPCs differentiated from BMSCs transfected with the miR-22-3p inhibitor did not show significant differences in size (Figure 2A and B). Interestingly, NPCs derived from miR-22-3p knockdowned BMSCs generated more neurospheres without IGF-1 supplementation (Figure 2C). Of note, the expression of miR-22-3p remained downregulated after neural induction (Figure 2D). This finding suggests that miR-22-3p inhibition had a similar effect as IGF-1 supplementation.

The effect of miR-22-3p inhibition on NPC proliferation was quantified using the MTS assay. Cellular proliferation of NPCs derived from miR-22-3p knockdowned BMSCs supplemented with EGF + bFGF and EGF + bFGF + IGF-1 both showed enhanced proliferation compared with

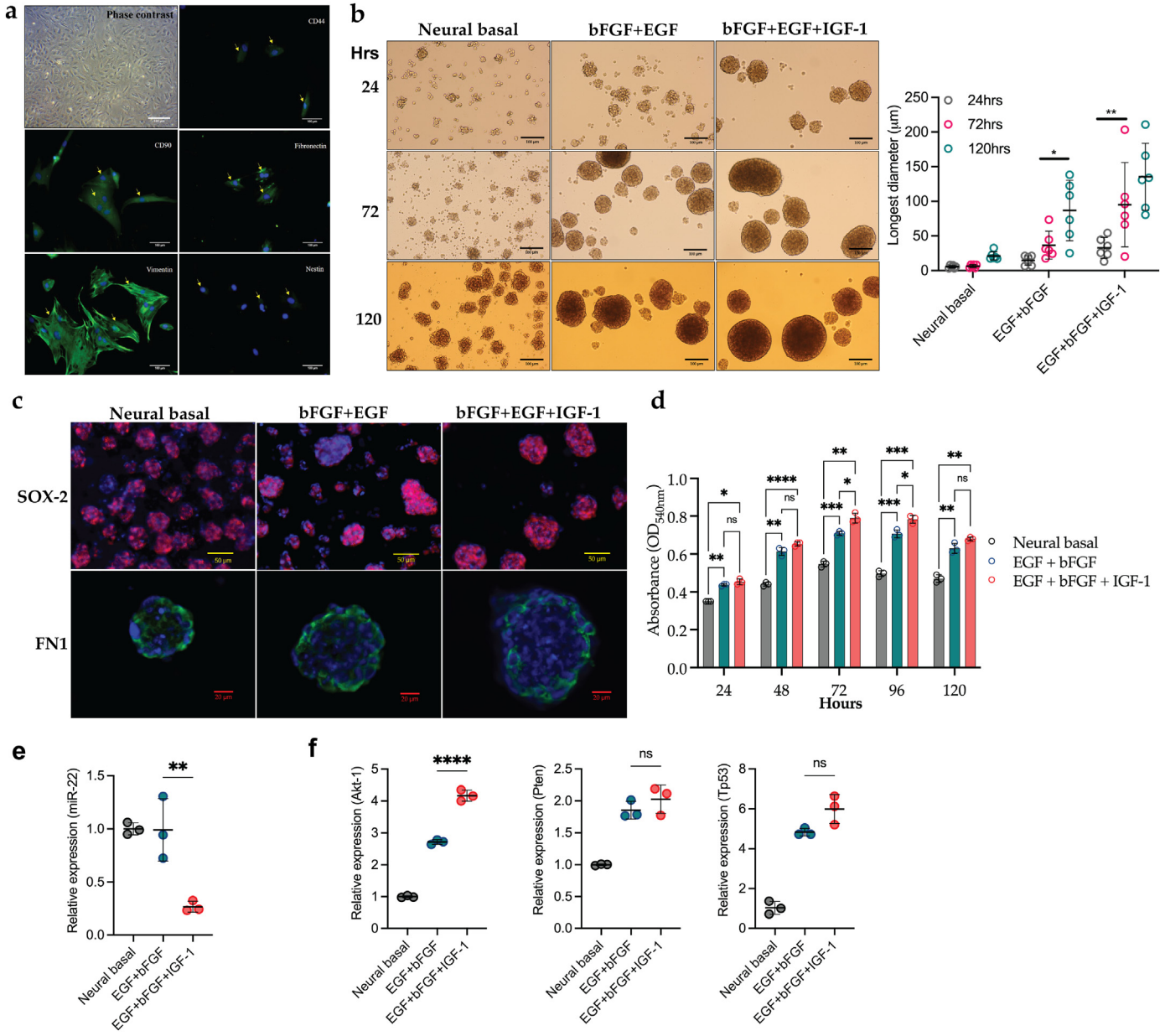

Figure 1. Supplementation of EGF, bFGF, and IGF-1 enhanced the cellular proliferation of BMSC-derived NPCs via downregulation of miR-22-3p. (A) Representative photomicrograph of BMSCs in culture. Immunocytochemical staining indicated that BMSCs expressed CD90, CD44, fibronectin, vimentin, and nestin. Nuclei were counterstained with Sytox Blue. Images were viewed under a confocal microscope. Scale bar: 100 µm. **(B)** Photomicrograph of free-floating neurospheres generated in neurobasal media with and without growth factor supplementation. Scale bar: 100 µm. The size of each neurosphere was measured using ImageJ based on the longest diameter. **(C)** Immunofluorescence staining of NPCs with Sox2 (scale bar: 50 µm) and fibronectin (scale bar: 20 µm). **(D)** Proliferation analysis of NPCs under different growth factors. Cells were incubated with an MTS reagent for 4 h, and changes in proliferation were studied at different time intervals. Data are represented as the mean optical density (OD) at 540 nm. **(E)** Expression level of miR-22-3p in BMSC-derived NPCs relative to the control (without growth factor). **(F)** Relative expression of the *Pten*, *Akt1*, and *Tp53* genes in NPCs derived from different growth factor combinations compared with the control. The indicated fold-change values were normalized to the *Actb* and *Gapdh* controls. All experiments were repeated in three biological replicates. Data are presented as mean ± SD. Statistical analysis was performed using one-way ANOVA. *$p < 0.05$, **$p < 0.01$, ***$p < 0.001$, and ****$p < 0.0001$.

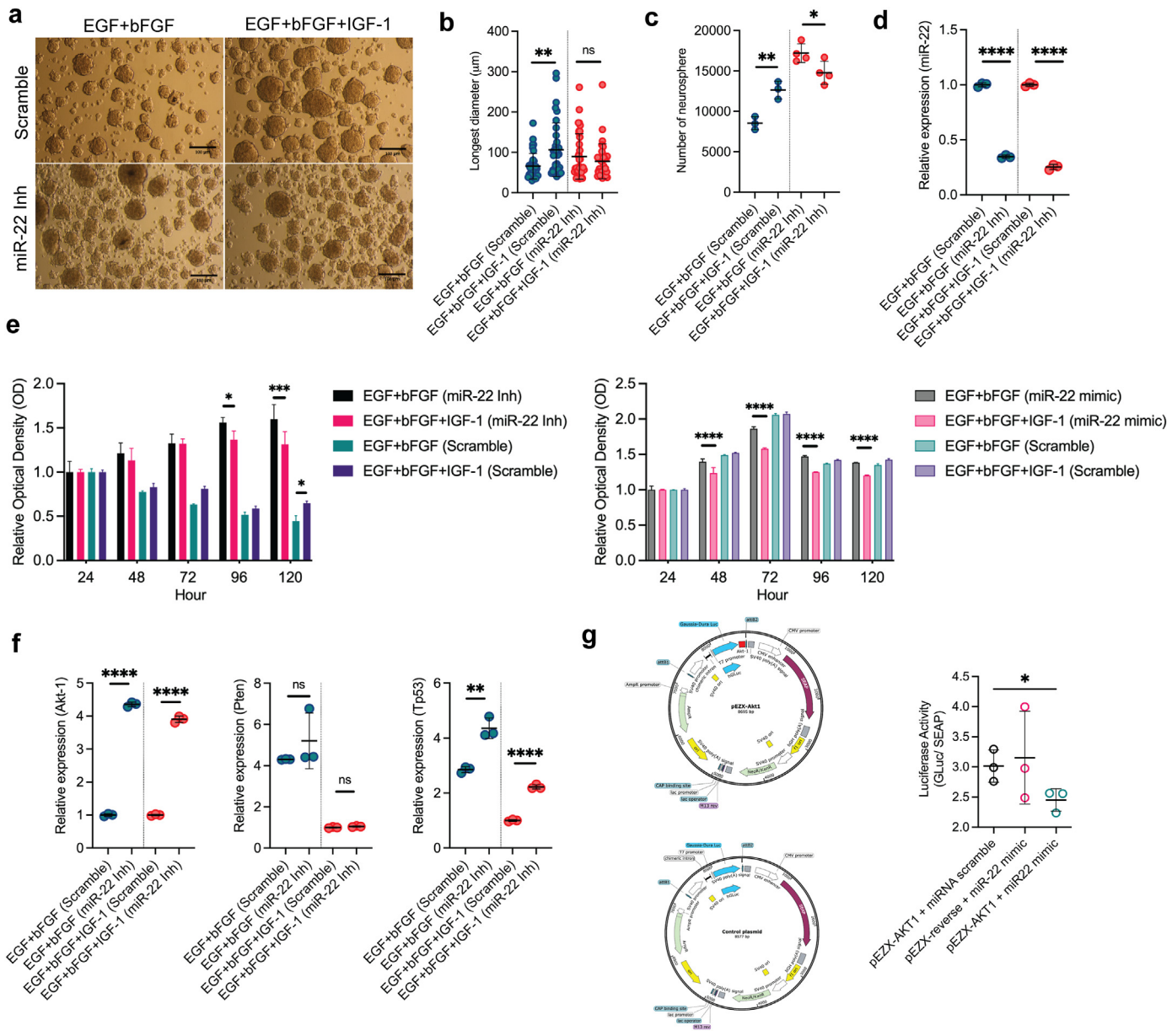

Figure 2. MiR-22-3p negatively regulated *Akt1* expression in promoting the cellular proliferation of BMSC-derived NPCs. (A) Representative photomicrographs of neurosphere-like cells generated from transfected BMSCs. BMSCs were transfected with either a microRNA inhibitor negative control (scrambled) or an miR-22-3p inhibitor (miR22-Inh). Transfected BMSCs were induced into a neural lineage under serum-free conditions supplemented with respective growth factor combinations. Images were viewed under an inverted light microscope. Scale bar: 100 μm. **(B)** Size of neurospheres based on the longest diameter. **(C)** Number of neurospheres in each condition. **(D)** Validation of miR-22-3p expression in NPCs derived from miR-22-3p knockdowned BMSCs. The control group was derived from BMSCs transfected with a scrambled microRNA hairpin inhibitor. **(E)** Cellular proliferation of BMSC-derived NPCs treated with the miR-22-3p inhibitor, miR-22-3p mimic, or scramble control. **(F)** The mRNA expression of *Akt1*, *Pten*, and *Tp53* was detected using qPCR. The expression was relative to the control group transfected with a scrambled inhibitor. **(G)** A luciferase reporter assay was conducted to demonstrate *Akt1* as a direct target of miR-22-3p. Data are presented as the ratio of the luminescence intensities (relative light unit, RLU) of the GLuc/SEAP expression. Experiments were repeated in three biological replicates. Data are presented as mean ± SD. Statistical analysis was performed using either the Student's t-test or one-way ANOVA. $*p < 0.05$, $**p < 0.01$, $***p < 0.001$, and $****p < 0.0001$.

their respective controls (Figure 2E). Consistent with the observed morphology, miR-22-3p knockdowned NPCs (EGF + bFGF) exhibited a higher proliferative activity than miR-22-3p knockdowned NPCs (EGF + bFGF + IGF-1). The differences are most prominent on days 4 and 5. Next, to confirm the anti-proliferative effect of miR-22-3p, a gain-of-function experiment was performed by transfecting BMSCs with miR-22-3p mimic and scramble control followed by neural induction. Interestingly, NPCs transfected with the scramble control exhibited a higher proliferative activity than the miR-22-3p mimic transfected group.

To elucidate the interaction between the predicted genes and miR-22-3p knockdown, the effect of miR-22-3p inhibition on the expression of *Akt1*, *Pten*, and *Tp53* was assessed using qPCR (Figure 2F). Knockdown of miR-22-3p in both groups showed upregulated expression of *Akt1* and *Tp53* genes but not *Pten*. The expression of *Akt1* and *Tp53* was decreased slightly in the presence of IGF-1. This finding supports our hypothesis that miR-22-3p is involved in fine-tuning cellular proliferation via the *Akt1* signaling pathway.

To confirm that miR-22-3p is a direct regulator of *Akt1*, the 3′UTR sequence of *Akt1* was cloned into a luciferase vector and transfected into BMSCs (Figure 2G). Co-transfection of the miR-22-3p mimic and plasmid containing the *Akt1* 3′UTR sequence resulted in a significant reduction of luciferase expression (2.452 ± 0.11 RLU, $p < 0.05$) compared with the

control with the reversed sequence (3.154 ± 0.44 RLU) and scrambled microRNA (3.016 ± 0.16 RLU) (Figure 2G). These data confirm that *Akt1* is a direct target gene of miR-22-3p.

2.3. Bulk RNA sequencing analysis of BMSC-derived NPCs

Next, we sought to understand how EGF, bFGF, and IGF-1 supplementation influenced the gene expression profile of BMSC-derived NPCs. We performed bulk RNASeq to compare the transcriptomic profile between BMSC-derived NPCs and undifferentiated BMSCs. To unveil the influence of IGF-1 supplementation, we also compared the transcriptomic profiles of NPCs derived with and without the presence of IGF-1. Assessment of similarity between replicates using principal component analysis (Figure 3A) and unsupervised hierarchical clustering using a distance matrix (Figure 3B) revealed that the BMSC-derived NPCs and BMSCs were well separated and that the samples clustered together,

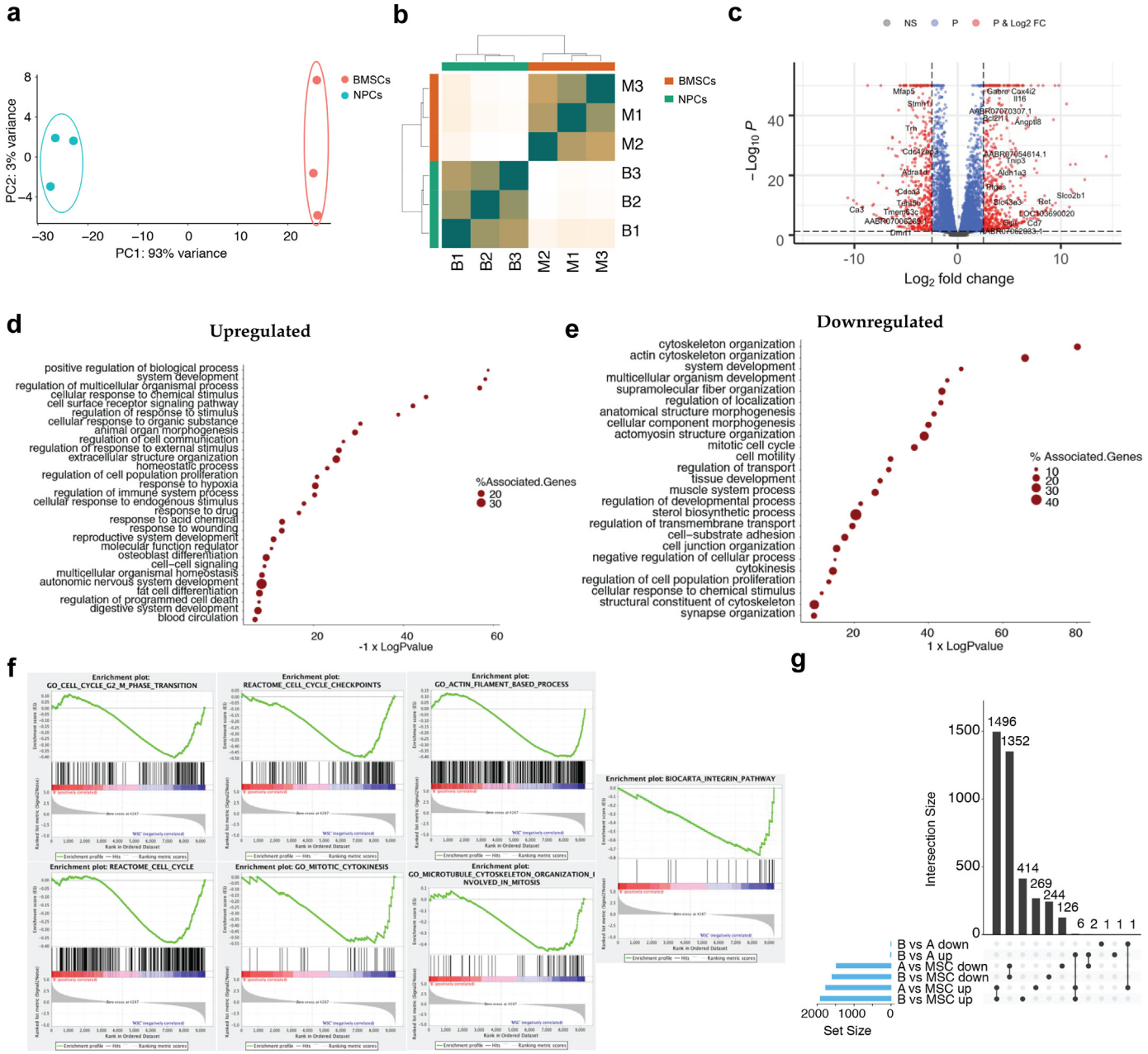

Figure 3. RNA sequencing comparing NPCs (EGF + bFGF + IGF-1) and BMSCs revealed a gene list associated with nervous system development (N = 3 per group). (A) Principal component analysis plot showing the separation of BMSC-derived NPCs from the BMSCs. **(B)** Unsupervised hierarchical cluster showing NPC replicates clustered together and separated from BMSCs. **(C)** Volcano plot illustrating the differentially expressed (DE) gene for each comparison between NPCs and BMSCs. Cut-off values of 0.05 and 2.0 are used for the *p*-value and fold change, respectively. Significant DE genes were annotated. *p*-values are capped at 50 for a maximized view. **(D-E)** Gene ontology (GO) terms enriched in genes upregulated **(D)** and downregulated **(E)** in NPCs. Significantly enriched (right-sided hypergeometric test) GO terms are shown in the y-axis, and the corresponding adjusted *p*-values (Bonferroni step-down) are reported in the x-axis. The sizes of the dots represents the percentages of genes associated with the GO term identified. **(F)** Gene set enrichment. Significantly enriched gene sets from MSigDB are reported for the gene expression analysis of NPCs compared with BMSCs. All the terms shown are upregulated in BMSCs. **(G)** UpSet plot of intersection across the three comparisons. The bar chart on the left indicates the total number of genes for each comparison separately for up and downregulated genes. The upper bar chart indicates the intersection size between sets of genes that are up or downregulated with one or more comparisons. The dark connected dots on the bottom panel indicate which comparisons are considered for each intersection.

corresponding to the group. The pairwise transcriptomic comparison of NPCs derived with EGF, bFGF, and IGF-1 revealed 3,513 differentially regulated genes, with 1,917 genes being upregulated and 1,596 genes being downregulated compared with the BMSCs.

The top 20 significantly differentially expressed protein-coding genes between NPCs (EGF + bFGF + IGF-1) and BMSCs are listed in Table 1. A complete list of the differentially expressed gene is provided in Table S3. The volcano plot demonstrates the significance and magnitude of expression changes, with some representative genes are labeled (Figure 3C).

All genes differentially regulated 2-folds and above were analyzed for GO terminology (Table S4). Non-redundant GO enrichment analysis in the upregulated genes revealed that 30% of the genes were enriched in the GO term autonomic nervous system development, indicating that the genes related to nervous system development are upregulated during differentiation (Figure 3D). On the other hand, the GO terms enriched in the downregulated genes were related mainly to cytoskeletal proteins (Figure 3E). A complete list of the upregulated genes involved in the GO terms, such as the nervous system, neurogenesis, and neuronal projection, is presented in Table S4. Furthermore, gene set enrichment analysis indicated that processes related to cell cycle regulation and mitotic cytokinesis, which are crucial during cell proliferation, were enriched in BMSCs on the expression dataset of NPCs versus BMSCs (Table 2 and Figure 3F).

Next, we compared the transcriptomic profiles of NPCs (EGF + bFGF + IGF-1) with those of NPCs (EGF + bFGF), which were reported earlier (Khan et al., 2020). Interestingly, only 11 differentially regulated protein-coding genes were identified between NPCs derived with and without IGF-1 (Table 3 and Table S5). Of note, WD repeat-containing protein 62 (*Wdr62*) and RET proto-oncogene were upregulated by 6.394-folds and 2.448-folds, respectively, in NPCs derived with IGF-1. Furthermore, assessment of the common and uniquely differently expressed genes across all the comparisons (Figure 3G) revealed some overlapping between differentially expressed genes (Jaccard score = 0.42), the upregulated genes of NPCs (EGF + bFGF) versus BMSCs and NPCs (EGF + bFGF + IGF1) versus BMSCs (Jaccard score = 0.41), and between the downregulated genes of NPCs (EGF + bFGF) versus BMSCs and NPCs (EGF + bFGF + IGF1) versus BMSCs (Jaccard score = 0.44). Despite the considerable overlaps, the transcriptomes of the two NPCs (derived with or without IGF-1) are distinct.

Table 1. List of top 20 differentially expressed gene.

Ensembl ID	Gene symbol	Log2 Foldchange	Adjusted P-value
ENSRNOG00000021201	*Txnip*	7.15	0.00E + 00
ENSRNOG00000015505	*Mfap5*	−5.19	0.00E + 00
ENSRNOG00000011490	*Angptl8*	6.79	1.02E − 28
ENSRNOG00000007827	*Cox4i2*	6.39	1.16E − 127
ENSRNOG00000029342	*Scn7a*	7.09	1.40E − 08
ENSRNOG00000056151	*Rasgrf2*	7.86	1.90E − 07
ENSRNOG00000021260	*Prnd*	−9.21	2.05E − 10
ENSRNOG00000005906	*LOC103690020*	8.75	2.30E − 09
ENSRNOG00000033026	*Dclk3*	6.14	2.42E − 08
ENSRNOG00000008245	*Ptgis*	5.59	3.31E − 31
ENSRNOG00000014333	*Vcam1*	5.87	3.40E − 53
ENSRNOG00000017976	*Slco2b1*	11.17	5.09E − 16
ENSRNOG00000052070	*Aldh1a3*	5.33	5.53E − 42
ENSRNOG00000007865	*Ephb1*	7.92	5.65E − 07
ENSRNOG00000011334	*Tmem63c*	−5.50	5.96E − 11
ENSRNOG00000014751	*Ret*	8.45	6.74E − 15
ENSRNOG00000032178	*Cenpa*	−6.71	6.84E − 10
ENSRNOG00000011989	*Vat1l*	7.54	9.03E − 09
ENSRNOG00000010079	*Ca3*	−9.79	9.38E − 12
ENSRNOG00000047349	*AABR07006269.1*	−5.98	9.79E − 08

Table 2. List of pathways and biological processes. Reported are the terms significantly enriched in BMSCs.

MSigDB Gene Set	SIZE	ES	NES	FDR q-value
INTEGRIN PATHWAY	19	−0.77	−2.01	0.00
CELL CYCLE CHECKPOINTS	160	−0.49	−1.86	0.00
ACTIN FILAMENT BASED PROCESS	435	−0.40	−1.68	0.03
CELL CYCLE	343	−0.38	−1.58	0.04
MITOTIC CYTOKINESIS	32	−0.55	−1.56	0.04
MICROTUBULE CYTOSKELETON ORGANIZATION INVOLVED IN MITOSIS	66	−0.46	−1.55	0.04
CELL CYCLE G2/M PHASE TRANSITION	162	−0.41	−1.55	0.03

ES = Enrichment score; NES = Normalised enrichment score; FDR = False discovery rate.

2.4. Terminal differentiation of NPCs on collagen hydrogel and electrophysiology

Next, we seeded NPCs generated under respective growth factor supplementations onto a collagen hydrogel matrix to mimic the 3D environment of the brain (Akcay and Luttge, 2021). Interestingly, NPCs from both groups differentiated into cells with neuronal features with elongated dendrites upon removal of growth factors and were cultured in the specialized NeuroCult™ NS-A differentiation media (Figure 4A). Differentiated cells exhibited pyramidal shapes with multiple neurite formations (Figure 2A Inset) and positively expressed beta-III-tubulin (TUJ1) and postsynaptic density protein 95 (PSD95) markers (Figure 4B). Notably, neurite protrusion and long neurite outgrowth were observed in both conditions but with more prominence on NPCs induced with EGF + bFGF + IGF-1. The formation of a synaptic junction-like structure was also observed between two differentiated cells (Figure 4C).

Next, we investigated the synaptic characteristics of neuronal-like cells using voltage clamps. The miniature excitatory postsynaptic current revealed that neuronal-like cells derived from the NPCs (EGF + bFGF + IGF-1) exhibited higher amplitudes than the current traces recorded in the neuronal-like cells from NPCs derived only with EGF and bFGF (Figure 4D). These data suggested that neuronal-like cells differentiated from the MSC-derived NPCs were functional.

2.5. Recovery of SCI promoted by BMSC-derived NPCs

We studied next the effects of BMSC-derived NPC transplantation on the recovery of the spinal cord after a hemisection injury (Figure 5A). Both NPCs derived under growth factor supplementation were transplanted into the spinal cord lesion. The Basso, Beattie, and Bresnahan (BBB) locomotor rating scale was used to assess locomotor function after SCI in rats (Figure 5B). The results showed that the recovery of sequential hind limb motor recovery was elicited in all treated groups except the sham and vehicle control groups (Figure 5C). Rats transplanted with

Table 3. Differentially expressed genes comparing between NPCs derived with and without IGF-1.

Ensembl	Genes symbol	Log2 FoldChange	Adjusted P-value
ENSRNOG00000013250	*Pdcd5*	*8.825*	*8.4E − 07*
ENSRNOG00000049708	*Wdr62*	*6.394*	*1.3E − 02*
ENSRNOG00000014751	*Ret*	*2.448*	*3.2E − 06*
ENSRNOG00000053272	*Chi3l1*	*1.404*	*4.3E − 02*
ENSRNOG00000007827	*Cox4i2*	*1.253*	*9.9E − 06*
ENSRNOG00000026605	*Ifi27l2b*	*1.233*	*1.8E − 02*
ENSRNOG00000003984	*Apln*	*1.212*	*1.4E − 07*
ENSRNOG00000061639	*AABR07044404.1*	*1.203*	*1.0E − 02*
ENSRNOG00000003244	*Ltc4s*	*1.118*	*5.2E − 03*
ENSRNOG00000020025	*LOC108348052*	*−1.400*	*3.4E − 03*
ENSRNOG00000046667	*Fosb*	*−1.770*	*4.8E − 18*

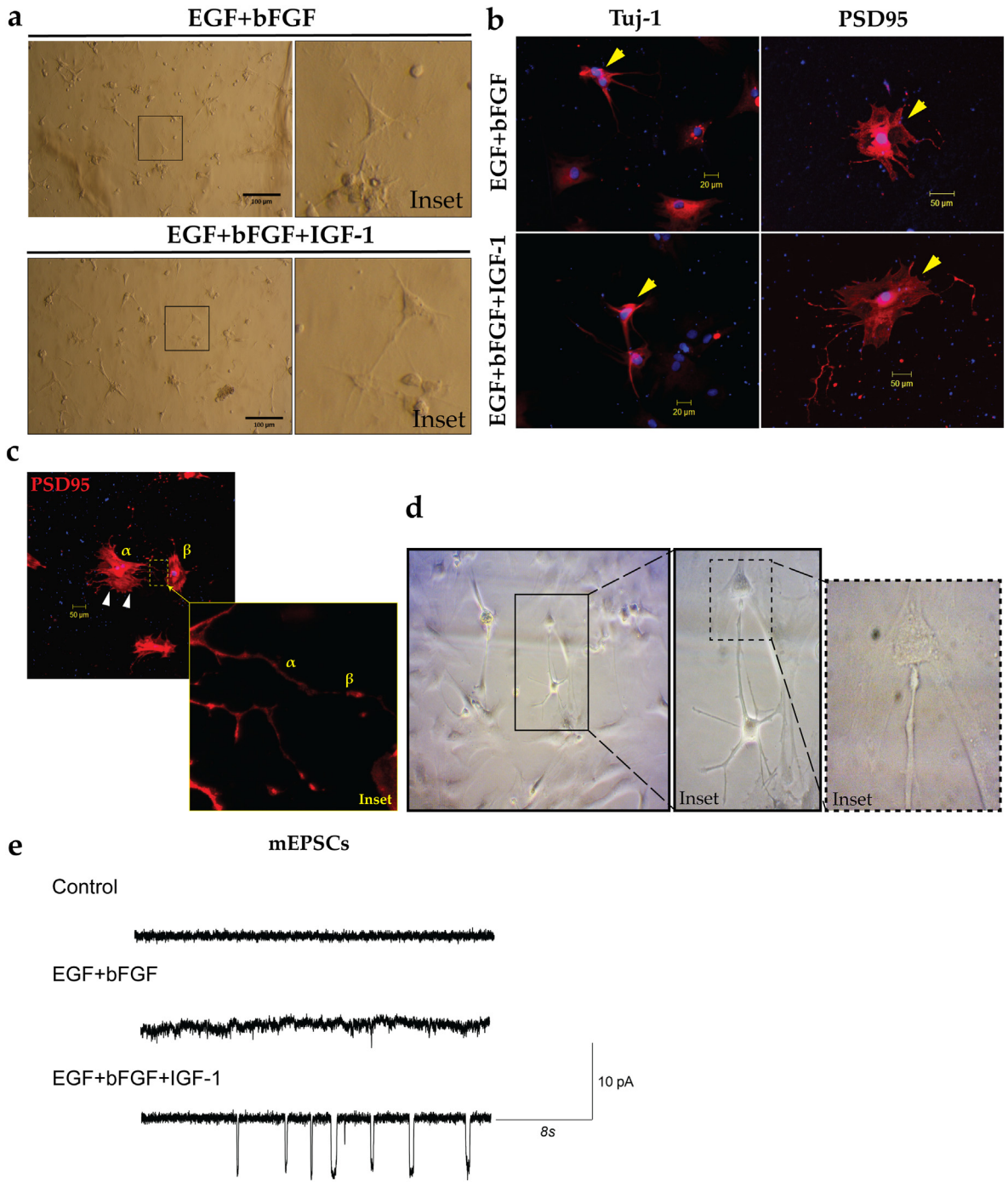

Figure 4. Terminally differentiated BMSC-derived NPCs exhibited neuronal-like phenotypes. (A) Representative photomicrograph of terminally differentiated BMSC-derived NPCs on a 3D collagen hydrogel. NPCs from both groups differentiated into neuronal-like cells. Images were viewed under an inverted light microscope. Scale bar: 100 μm. **(B)** Representative image of neuronal-like cells expressing neuronal markers, such as TUJ1 and PSD95. NPCs derived under the supplement of IGF-1 differentiated into neuronal-like cells with longer neurites. Scale bar: 50 μm. **(C)** Close-up image of neurite outgrowth from NPCs (EGF + bFGF + IGF-1). Neurite protrusions (white triangle) and elongated neurites (inset) were observed after 1 week in culture. Scale bar: 50 μm. **(D)** Representative phase-contrast image of neuronal-like cells used for patch clamp recording. **(E)** Representative traces of spontaneous miniature excitatory postsynaptic current recorded. Cells in both groups produced spikes with larger amplitudes than thoseof the control. Undifferentiated cells, assumed to be glial cells, served as controls during patch clamp recording. Experiments were repeated thrice independently.

NPCs (EGF + bFGF + IGF-1) performed the best, recording the highest mean BBB scores of approximately 12 at day 28 post-transplantation. By contrast, the rats transplanted with NPCs derived without IGF-1 supplementation achieved stabilized mean BBB scores of roughly 9.

Mechanical sensory function was assessed using Von Frey filaments. The starting filament was used at a force of 2 g. There were no differences in the paw withdrawal threshold before injury and at day 1 post-transplantation among all groups (Figure 5D). However, starting from day 7 post-transplantation, the average values of the paw withdrawal threshold in animals with NPCs (EGF + bFGF + IGF-1) were significantly reduced compared with those of the group receiving NPCs (EGF + bFGF), $p < 0.05$. These data suggested that transplantation of NPCs derived under IGF-1 supplementation promoted both locomotor and sensory recoveries of SCI.

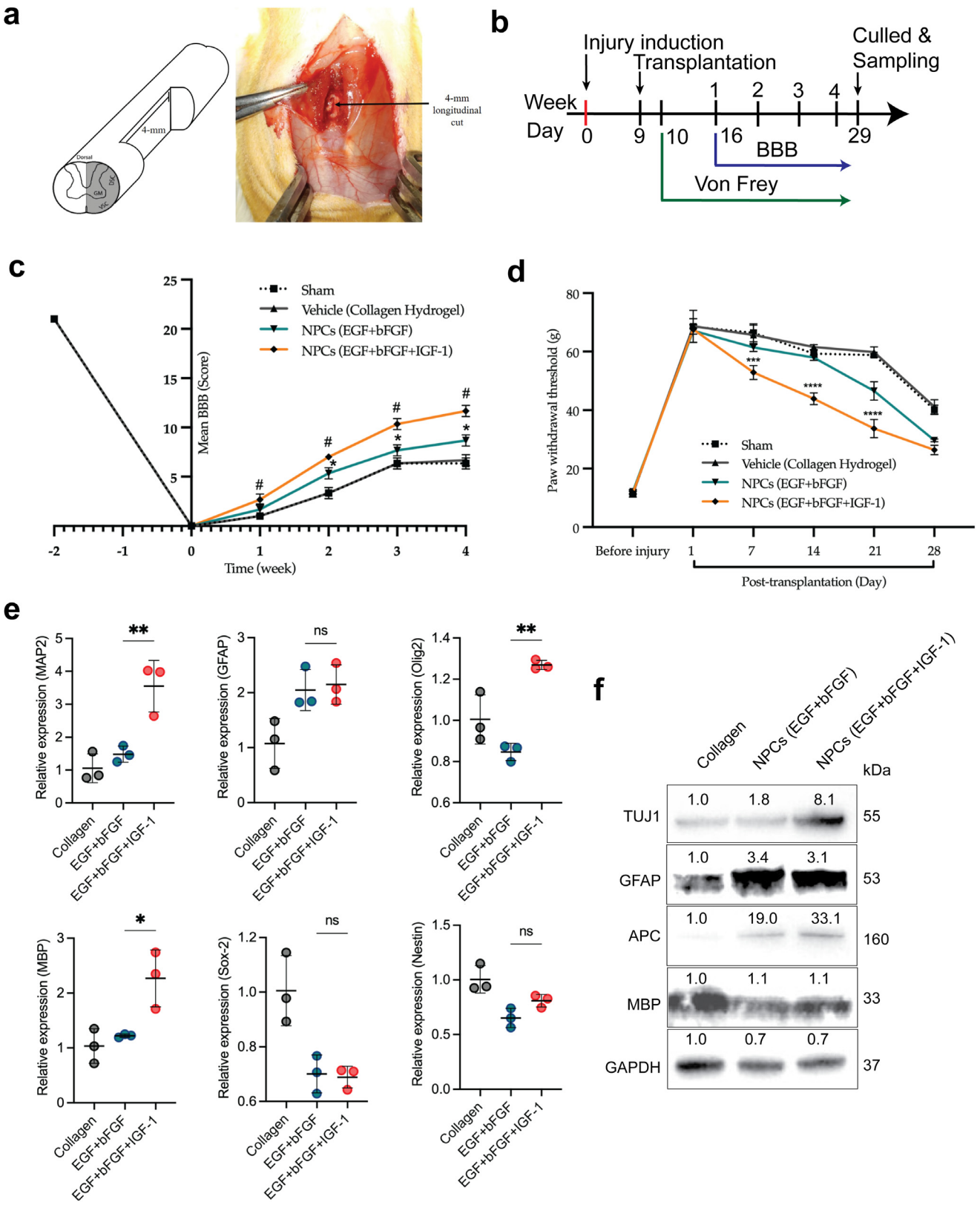

Figure 5. Transplantation of BMSC-derived NPCs in a spinal cord injury animal model promoted locomotor and sensory recoveries (N = 3 per group). (A) A 4-mm-long longitudinal cut along the midline of the spinal cord for lateral hemisection at the T9-T10 level. **(B)** Timeline of the entire in vivo transplantation study. **(C)** Open-field locomotor assessment. The hind limb function of all rats was assessed using the Basso, Beattie, and Bresnahan (BBB) locomotor scale. **(D)** Mechanical sensory assessment as conducted with the Von Frey filament test. Two-way ANOVA was performed, followed by a Tukey test to compare the mean difference among the groups and times. An asterisk (*) indicates a significant difference of the treatment groups and the control group. A hashtag (#) indicates a significant difference between treatment days. **(E)** Relative expression of *Map2, Gfap, Olig2, Mbp, Sox2*, and nestin within the transplanted region of the spinal cord. **(F)** Western blot analysis and relative quantification of TUJ1, GFAP, APC, and MBP. Each protein band was normalized to GAPDH. Data are presented as mean ± SD. Statistical analysis was performed using one-way ANOVA to compare within groups. $^{*}p < 0.05$, $^{\#}p < 0.05$, $^{***}p < 0.001$, and $^{****}p < 0.0001$.

We subsequently investigated the impact of stem cell transplantation on gene and protein expression within the transplanted region. Gene expression of neurons (*Map2*), astrocytes (*Gfap*), oligodendrocytes (*Olig2*), myelination (*Mbp*), and neural stem cells (nestin and *Sox2*) was quantified using qPCR (Figure 5E). Animals receiving NPCs (EGF + bFGF + IGF-1) exhibited significantly higher *Map2*, *Mbp*, and *Olig2* than those animals receiving NPCs (EGF + bFGF). Moreover, *Gfap* expression was also increased in the animals transplanted with NPCs (EGF + bFGF + IGF-1), but they showed no significant differences compared with the animals receiving NPCs (EGF + bFGF). There was no significant difference in the level of stem cell markers, nestin and *Sox2*, in both NPC transplanted groups. These data suggested that transplanted NPCs have differentiated into neurons, astrocytes, and oligodendrocytes. Furthermore, a higher *Mbp* expression in animals receiving NPCs (EGF + bFGF + IGF-1) meant better re-myelination of the spinal cord in this group of animals. Western blot analysis showed that markers for neuronal cells (TUJ1), glial cells (GFAP), and Oligodendrocytes (APC) were expressed after NPC transplantation (Figure 5F). Animals transplanted with NPCs (EGF + bFGF + IGF-1) exhibited the highest expression of TUJ1 and APC consistent with the gene expression. These data suggested that NPCs derived under the influence of EGF + bFGF + IGF1 had a higher tendencies to differentiate into neuronal and glial cells compared with NPCs (EGF + bFGF).

To observe the effect of NPC transplantation in the cross-sectioned area of the injured spinal cords, tissues from the adjacent site of the lesion area were sectioned at 3 μm thickness at day 28 post-treatment. The recovery was minimal in the vehicle control group, in which the animals received only collagen hydrogel, with poorly developed neurons and some glial cells present in the gray matter. The white matter showed extensive microcyst formation and marked necrosis, as evidenced by perinuclear cytoplasmic vacuolation of the glial cells (Figure 6A).

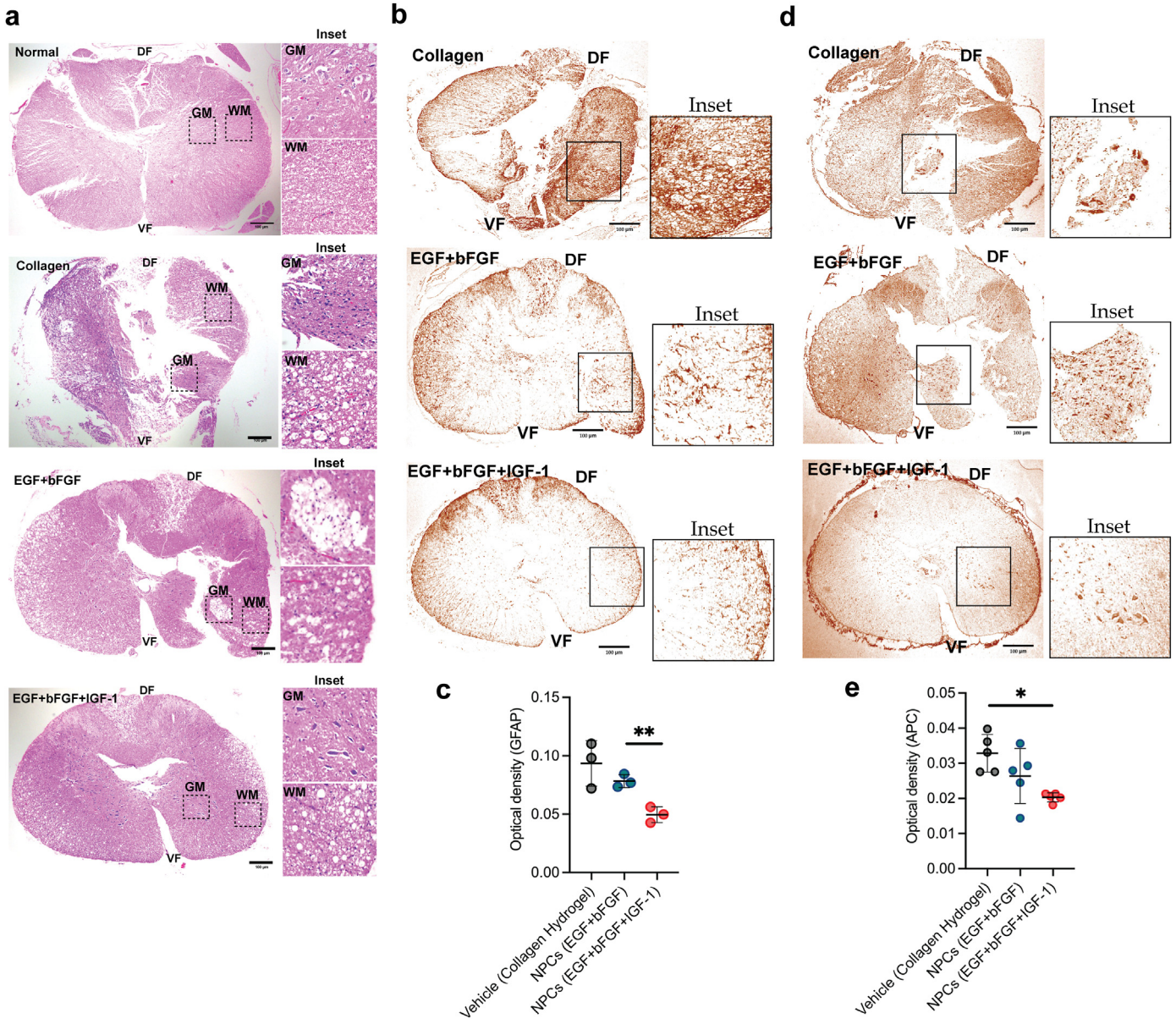

Figure 6. Animals transplanted with NPCs (EGF + bFGF + IGF-1) exhibited less inflammation in the tissues adjacent to the lesioned site (N = 3 per group). **(A)** Hematoxylin and eosin (H&E) staining of the gray and white matter sections of the spinal cord. **(B-E)** Immunohistochemistry staining of spinal cord sections against GFAP **(B)** and APC **(D)** markers. The mean intensity of GFAP (C) and APC (E) staining was analyzed using the IHC toolbox/Deconvolution function plugin from ImageJ. Optical density (mean gray value) obtained using color deconvolution and computerized pixel profiling led to automated scoring. The final score was shown in the corrected OD value (background deducted), which represents the intensity of the brownish color; where the darker the brownish color, the higher the OD value. Scale bar: 100 μm. Data are presented as mean ± SD. Statistical analysis was performed using one-way ANOVA to compare within groups. $*p < 0.05$, $**p < 0.01$.

Furthermore, a noticeably higher number of immune cells infiltrated indicated a greater severity of inflammation. A few neurons and more astrocytes appeared in the gray matter in the vehicle group. Still, the white matter showed extensive microcyst formation and the presence of only a few astrocytes. In animals receiving NPCs (EGF + bFGF), microcysts and vacuolation were still present in the white matter. The profile of tissue healing was significantly improved in animals receiving NPCs (EGF + bFGF + IGF-1). Although vacuolation was still present, the severity was lesser than in animals receiving NPCs (EGF + bFGF), and the tissue structure was more compact and well formed.

Microcyst formation and inflammatory cells were not observed in this group. We also found that animals receiving NPC transplantation exhibited a lower expression of GFAP than the vehicle control at the adjacent site of the lesion (Figure 6B and C). By contrast, spinal cord transplanted with NPCs showed more APC-positive cells (Figure 6D and E). These data suggested that NPC treatment could have an anti-inflammatory effect while promoting motor and sensory recovery through re-myelination.

3. Discussion

We have elucidated the molecular mechanism underlying the growth factors-induced neural differentiation of BMSCs. Supplementation of EGF, bFGF, and IGF-1 enhanced cellular proliferation and survivability through downregulation of miR-22-3p. The derived NPCs can differentiate terminally into cells exhibiting neuronal-like phenotypes. Moreover, RNASeq analysis unveiled a series of upregulated genes involved in neural differentiation and development, whereas genes involved in BMSC proliferation were downregulated. Intriguingly, transplantation of BMSC-derived NPCs promoted the recovery of the injured spinal cord in a rat model.

BMSCs have been reported to differentiate into NPCs under growth factor supplementation. The combination of EGF and bFGF is commonly used to differentiate BMSCs into free-floating aggregates called neurospheres (Chouw et al., 2020; Mung et al., 2016). In our earlier study, we reported that the addition of IGF-1 synergistically with EGF and bFGF further enhanced the cellular proliferation and survivability of BMSC-derived NPCs (Huat et al., 2014). IGF-1 is locally produced in the brain and is essential during development (Wrigley et al., 2017; Nieto-Estévez et al., 2016). A study reported that IGF-1-mediated neurogenesis involved the RIT1/Akt/Sox2 cascase (Mir et al., 2017). IGF-1 stimulated an RIT1-dependent increase in Sox2 levels, which subsequently enhanced pro-neural gene expression and promoted cellular proliferation. However, the expression of IGF-1 decreased significantly in the brain upon neuronal maturation (Song et al., 2016). Conversely, IGF-1 and IGF-1R expression levels in the brain were reported to increase following traumatic brain injury (Mangiola et al., 2015). Exogenous administration of IGF-1 was also neuroprotective in ischemic brain injury (Serhan et al., 2019). Increased hippocampal levels of IGF-1 promoted end-stage maturity of post-trauma-born of neurons and improved cognition following injury (Littlejohn et al., 2020). However, one study reported that long-term IGF-1 treatment could induce epileptic and neurotoxicity (Song et al., 2016), so the risk of immediate treatment of IGF-1 needs to be carefully considered. In the present study, NPCs were induced *in vitro* in the presence of IGF-1. Healthy neurospheres were subsequently used as cell therapy, thus avoiding the unnecessary risk of growth factor oversupply.

An *in silico* analysis of microRNA profiles delineated several important microRNAs associated with cell proliferation and programmed cell death that were downregulated upon IGF-1 supplementation (Huat et al., 2015a). Among the aberrantly regulated microRNAs, miR-22-3p was the most strikingly downregulated. MiR-22-3p is a highly conserved microRNA with multiple functions, such as epigenetic modification (Kim et al., 2015b), cell differentiation (Zhao et al., 2015), tumorigenesis (Zuo et al., 2015), and disease development (Huang et al., 2013). According to the earliest studies on miR-22-3p, the role of this microRNA in cellular proliferation and apoptosis is context dependent. Under normal physiological conditions, miR-22 is widely expressed in all tissues (brain, heart, liver, lung, kidney, smooth muscle, prostate, testis, ovary, placenta, and adipose) and is associated with cellular differentiation and senescence (Xiong, 2012; Xu et al., 2011; Jazbutyte et al., 2013). It has been shown that miR-22 regulated smooth muscle cell differentiation by targeting MECP2, whereas knockdown of miR-22 inhibited the differentiation (Zhao et al., 2015). Overexpression of miR-22-3p also decreased the cellular proliferation of cerebellar granular neuron precursors by targeting Max. By contrast, knockdown of miR-22-3p diminished the anti-proliferative activity of bone morphogenetic protein 2, causing the cell to proliferate (Berenguer et al., 2013).

On the other hand, miR-22 expression is commonly downregulated in cancer cell lines and is associated with uncontrolled metastasis (Xu et al., 2014; Yang et al., 2014; Xu et al., 2011). Suppression of miR-22 enhanced the cellular proliferation of tongue squamous cell carcinoma by regulating CD147 expression (Qiu et al., 2016). A similar effect of miR-22 inhibition was reported in hepatocellular carcinoma (Luo et al., 2017) and breast cancer cell lines (Kong et al., 2014). Moreover, overexpression of miR-22 has been reported to inhibit the cellular proliferation and migration of glioblastoma by targeting the SIRT1 expression (Chen et al., 2016). These studies proved that the miR-22-3p had various effects, which were context based.

BMSC-derived NPCs under IGF-1 supplementation showed higher *Akt1* expression than the NPCs (EGF + bFGF) did, consistent with the enhanced cellular proliferation of NPCs observed in the presence of IGF-1. IGF-1 has been reported to activate the PI3K/AKT and MAP kinase signaling pathways, which confer neuroprotective effects (Wang et al., 2015). Bindings of IGF-1 to IGF-1R activated the receptor kinase, which phosphorylated various intracellular proteins, such as insulin receptor substrate-1 and Shc, leading to the activation of multiple pathways, including PI3K/AKT and MAPK (Laviola et al., 2007). The administration of IGF-1 has been reported to induce cellular proliferation of cultured myoblasts via the PI3K/AKT signaling pathway (Yu et al., 2015). All these evidences highlight the role of IGF-1 in promoting cell proliferation and survival.

Our study demonstrated the ability of miR-22-3p to inhibit *Akt1* expression and proposed a mechanism of post-transcriptional regulation of the *Akt1* gene. Co-transfection of the luciferase vector containing a wild-type 3′UTR sequence of *Akt1* and miR-22-3p mimic resulted in a significant reduction in luciferase activity, proving the inhibition of *Akt1* translation by miR-22-3p. Accumulating evidence reports that the *Akt1* gene directly targeted by microRNAs, such as miR-143 and miR-302a, resulted in the growth inhibition of cancer cells (Zhang et al., 2015; Noguchi et al., 2013). By contrast, downregulation of the miR-99 family has been reported to release *Akt1,* which activates cell proliferation and migration via the PI3K/AKT pathway (Jin et al., 2013). Our study suggested that miR-22-3p could directly target and regulate the post-transcription of *Akt1* in BMSC-derived NPCs upon IGF-1 supplementation.

As reported in our earlier study, NPCs derived with IGF-1 were better than those derived without IGF-1 (Huat et al., 2014). In the present study, we found 11 differentially expressed genes between the two NPCs (Table 3). Among these genes, *Pdcd5 and Wdr62* were upregulated 256-folds and 64-folds, respectively. Programmed cell death 5 (*Pdcd5*) has been reported to regulate cell proliferation, cell cycle progression, and apoptosis (Li et al., 2018). A study reported that IGF-1 was inversely correlated with *Pdcd5* expression (Yi et al., 2013). An increased level of programmed cell death during neural induction is expected when not all cells undergo neural differentiation (Pang et al., 2021). Nevertheless, apoptotic MSCs could be beneficial, warranting further investigation.

WD40-repeat protein 62 (*Wdr62*) is a spindle microtubule-associated phosphoprotein that is crucial for maintaining neural and glial cell populations during brain development (Shohayeb et al., 2020a; Alshawaf et al., 2017). Knockout of *Wdr62* resulted in a significant reduction in the thickness of the hippocampal ventricular and dentate gyrus (Shohayeb

et al., 2020a). By contrast, overexpression of *Wdr62* has increased the cell proliferation and brain volume of the Drosophila larvae by activating pAKT signaling (Shohayeb et al., 2020b). The upregulation of the *Wdr62* gene may signify the role of this gene in specifying the intermediate neural progenitor during BMSC differentiation into a neural lineage.

For the functional study, we transplanted BMSC-derived NPCs in the subacute stage of SCI. Two complementary locomotor function and Von Frey filament tests showed that the transplanted NPCs could significantly improve motor recovery and sensory function for the affected hind limb, respectively. The animals receiving NPCs (EGF + bFGF + IGF-1) displayed higher average of BBB score compared with those animals receiving NPCs (EGF + bFGF) and the vehicle alone. In addition, the average values of the paw withdrawal threshold in the animals receiving NPCs (EGF + bFGF + IGF-1) were significantly reduced compared with the vehicle control. All these pieces of evidence suggested that NPCs (EGF + bFGF + IGF-1) can improve the recovery of SCI in rat model.

The histology of spinal cord tissues after hemisection of SCI was examined using hematoxylin and eosin (H&E) staining to elucidate possible mechanisms leading to the observed functional recovery. The spinal cord section of the control group revealed marked areas of necrosis with vacuolation within the white matter as a result of chronic accumulation of edema and protein aggregates (Wang et al., 2021). By contrast, spinal cord transplanted with NPCs had minimal residual lesions that were barely visible in the cross-section of the spinal cord, and the profile of tissue damage was far more improved. Immunohistochemistry (IHC) staining of the spinal cord using antibodies was examined to detect stemness (SOX2), neural precursor cells (NESTIN), astrocytes (GFAP), oligodendrocytes (APC), and myelin (MBP) 4 weeks after transplantation. Our IHC data showed that NPCs derived under EGF, bFGF, and IGF-1 could differentiate into myelin-forming cells in complex niches after transplantation in the injured spinal cord. This development of myelination has the highest intensity among the groups. The data suggested that BMSC-derived NPC transplantation promoted spinal cord recovery by increasing re-myelination at the lesioned site. Nevertheless, our study did not exclude the possibility that endogenous stem cells or MSC-derived exosomes could also play a role in overall recovery (Mu et al., 2022).

To examine the differentiation potential of NPCs transplanted in the lesioned region, we have evaluated the gene expression for stemness (*Sox2 and* nestin*),* neurons *(Map2)*, astrocytes (*Gfap),* oligodendrocytes *(Olig2),* and myelination (*Mbp)* using tissue within the transplanted region. Our results demonstrated a significant increase in *Map2*, *Olig2*, and *Mbp* gene expression in the spinal cords of animals receiving NPCs (EGF + bFGF + IGF-1) compared with those receiving NPCs (EGF + bFGF). *Gfap* expression was also increased in the NPC-treated groups compared with the vehicle control. It is well reported that oligodendrocytes are the myelinating cells of the CNS and play essential roles in the recovery of the injured spinal cord (Kuhn et al., 2019). Both stemness-related genes (*Sox2* and nestin) were not expressed in the NPC transplanted groups. Migrating NSCs at the lesioned side of the spinal cord were reported to change their morphology and lose expression of SOX2 expression (Meletis et al., 2008). Similarly, nestin is commonly used as a marker for NSCs and is essential for NSC self-renewal (Park et al., 2010). Within 24 h of differentiation initiation, neural stem progenitor cells lose their nestin expression, followed by an increased *Tuj1* expression (Kim et al., 2015a). Therefore, our data suggested that NPCs derived under IGF-1 supplementation could differentiate into neuronal or oligodendrocyte cell types.

We also evaluated the expression of TUJ1 (neuron), GFAP (astrocyte), APC (oligodendrocyte), and MBP (myelin) at the protein level. Animals receiving NPCs (EGF + bFGF + IGF-1) showed relatively higher expressions of TUJ1 and APC, consistent with the gene expression. The expression of APC indicated myelin sheath formation around the axon because oligodendrocytes are glial cells that support the CNS. They elongated into high numbers of branches and sub-branches, expanding into sheets of myelin membranes that wrapped around multiple neural axons. The myelin sheath accelerated rapid saltatory conduction and insulation of the nerve cells (Cohen et al., 2020). Furthermore, oligodendrocytes promoted neuronal and axonal survival by secreting different neurotrophic factors (Wilkins et al., 2003). The astrocyte marker (GFAP) was also expressed relatively higher in the NPC-transplanted groups. Astrocytes play important roles in sealing the lesion site in the early phase of neural damage (Okada et al., 2006). Studies have shown that astrocytes provide support and axonal guidance and aid in improving functional recovery after SCI (White and Jakeman, 2008). Intriguingly, a study reported that astrocytes can be reprogrammed into neurons in the injured spinal cord (Su et al., 2014). However, whether NPC-derived glial cells in this study contribute to the recovery warrant a further investigation.

In summary, our results suggested that IGF-1 supplementation, along with EGF and bFGF, enhanced the differentiation of BMSCs into NPCs in terms of cellular proliferation and survivability. We demonstrated the mechanism underlying the enhancement of NPC culture under the combination of EGF, bFGF, and IGF-1, which involved the miR-22-3p as a critical post-transcriptional regulator. This study presented incipient evidence that miR-22-3p was engaged in enhancing cellular proliferation and survivability of BMSC-derived NPCs under the influence of mitogens. Transplantation of NPCs in the SCI rat model promoted the recovery of sensory and motor functions. Our study has contributed significantly to the field and proposed that IGF-1 induced BMSC-derived NPCs are suitable candidates for stem cell therapy, especially in the treatment of SCI.

4. Limitations of the study

This study was limited by the inability to differentiate between transplanted NPCs and endogenous NPCs. Our initial attempt to tag the cells with fluorescence failed because of the high proliferation rate of stem cells, which resulted in the fading of the fluorescence signal. The instability of the fluorescence dye was another factor that contributed to the failure. A higher apoptotic rate was also observed in the tagged primary cells, significantly affecting the downstream experiments. Nevertheless, we believe that the therapeutic effects are the outcomes of transplantation because of the dormancy of endogenous neural stem cells. Still, we cannot rule out the contribution of endogenous neural stem cells in the overall recovery.

Declarations

Author contribution statement

Putri Nur Hidayah Al-Zikri: Conceived and designed the experiments; Performed the experiments; Analyzed and interpreted the data; Wrote the paper.

Tee Jong Huat: Conceived and designed the experiments; Performed the experiments; Analyzed and interpreted the data; Contributed reagents, materials, analysis tools or data; Wrote the paper.

Amir Ali Khan: Conceived and designed the experiments; Analyzed and interpreted the data; Contributed reagents, materials, analysis tools or data.

Azim Patar, Mohammed Faruque Reza: Analyzed and interpreted the data.

Fauziah Mohamad Idris, Jafri Malin Abdullah, Hasnan Jaafar: Conceived and designed the experiments; Contributed reagents, materials, analysis tools or data.

Funding statement

Hasnan Jaafar was supported by the Universiti Sains Malaysia Research University Grant (grant no: 1001/PPSP/812170).

Fauziah Mohamad Idris was supported by USM Research Grant (grant number: RUI/PPSP/1001/812148).

Tee Jong Huat was supported by the Malaysia Toray Science Foundation (grant no: 304/PPSP/6150142/M126).

Jafri Malin Abdullah was supported by a grant from Malaysian National Cancer Council (MAKNA).

Amir Ali Khan was supported by a Competitive Research Grant from the University of Sharjah (grant no: 1602145036-P).

Data availability statement

Data associated with this study has been deposited at NCBI under the accession numbers GSE104548 and GSE60060.

Declaration of interest's statement

The authors declare no conflict of interest.

Additional information

Supplementary content related to this article has been published online at https://doi.org/10.1016/j.heliyon.2022.e10384.

Acknowledgements

PNHA was supported by MyBrain15 from the Ministry of Education (Malaysia). TJH was supported with a fellowship from Universiti Sains Malaysia. MicroRNA microarray was carried out at the Human Genome Centre, USM. Flow cytometry was performed at the Department of Immunology, USM. We thank Mr Jamarruddin Mat Asan for technical assistance with flow cytometry studies. We thank all Integrated Centre for Animal Care and Use (ICRACU). We thank all members of the Department of Neuroscience, Department of Pathology, Department of Microbiology for their helping hands and supports.

Appendix

STAR methods

Resource availability

Lead contact

Further information and requests for resources and reagents should be directed to and will be fulfilled by the lead contact, Tee Jong Huat (teejonghuat@gmail.com).

Materials availability

This study did not generate new unique materials.

Data and code availability

- RNA sequencing and microRNA profiling data have been deposited at GEO database NCBI and publicly available with the accession number GSE104548 and GSE60060, respectively.
- Microscopy data reported in this paper will be shared by the lead contact upon request.
- This paper does not report original code.
- Any additional data required to reanalyze the data reported in this paper is available from the lead contact upon request.

Experimental model and subject details

Animal surgical procedure and postoperative care

Adult Sprague-Dawley (SD) rats were supplied by Animal Research and Service Centre, Universiti Sains Malaysia. The board of animal ethics committee of Universiti Sains Malaysia approved all experimental procedures involving animals performed in this study [USM/Animal Ethics Approval/2015/(96) (633)].

Female SD rats aged 8–12 weeks were anaesthetised by intraperitoneal ketamine (90 mg/ml) and xylazine (5 mg/ml). Body temperature was maintained around 37 °C by keeping the animal on a heating pad throughout the surgery. The rat's back was shaved and disinfected with an alcohol swab and iodine. The tenth thoracic (T10) vertebra was identified according to Medinaceli (1986), and muscle tissue was dissected to expose laminae T9-T11. A T10 laminectomy was performed, and the dura matter was removed. A lateral hemisection at the T10 level was accomplished by creating a 4 mm longitudinal cut along the midline of the cord with a 15° stab knife. Then, lateral cuts were made at the rostral and caudal ends to remove the tissue.

After surgery, the surgical site was closed by suturing the muscle and the skin using Catgut Chrom 4/0 (B|Braun, Germany). The sutured cut site was wiped with iodine. Animals remained on a heating pad until they regained consciousness and were placed back in their home cages. Bladders were manually expressed after the operation until needed. All post-care surgery was performed accordingly. All rats received analgesia of 1 mg/kg of Meloxicam (1 mg/kg) (INTAS, India) and antibiotic Baytril (5 mg/kg) (Bayer, Germany) via intramuscular injection daily for three days as suggested by the veterinarian. All animals were closely monitored for general health, infections, or autophagy of the toes for up to 2 weeks aftermath the surgery. None of the animals in the study showed any sign of infection or autophagy due to surgery.

Primary cell isolation and culture

BMSCs were isolated according to the protocol described earlier (Huat et al., 2014). Briefly, SD rats (4–6 weeks old) were sacrificed by overdose of ketamine (100 mg/ml) and xylazine (100 mg/ml) cocktail (Ilium Troy Laboratory, Australia). BMSCs were flushed out from the marrow cavity of both tibias and femoral bones and cultured in a complete media consisting of DMEM supplemented with 20% fetal bovine serum, 1% non-essential amino acid (100×), and 1% penicillin/streptomycin (10,000 U/ml) (Life Technologies, CA, USA). Cells were maintained in a humidified incubator at 37 °C with 5% CO_2 supplementation. On the following day, non-adherent cells were removed by total media replacement. Cells were monitored every day, and media was changed every 2–3 days until the primary colonies (passage 0, P0) of BMSCs became visible. BMSCs were cryopreserved at P2, and subsequence experiments were conducted using the stem cells at P4. We have never encounter any mycoplasma problem due to short term storage and used up of primary isolated BMSCs.

Method details

Phenotypic characterization and trilineage differentiation of BMSCs

BMSCs at P4 were used for characterization. Briefly, the BMSCs were fixed in 4% paraformaldehyde for 30 min and permeabilized with 1% Triton X-100 for 2 min. The cells were then blocked with a solution containing 1% bovine serum albumin, 10% normal donkey serum, and 0.3 M glycine for 1 h at room temperature. The cells were incubated overnight at 4 °C with the following primary antibodies: anti-CD44 (PE) conjugated rat monoclonal antibody (#ab25224, 1:200; Abcam, UK), anti-CD90 (FITC) conjugated mouse monoclonal antibody (#MA1-81572, 1:100; Thermo Scientific, USA), Alexa Fluor® 647 mouse anti-nestin (#560393, 1:200; BD Pharmingen, USA), anti-vimentin FITC conjugated antibody (#ab92547, 1:100; Abcam, UK), anti-CD11b (#ab25533, 1:50; Millipore, USA), and anti-fibronectin (#ab23751, 1:100; Millipore USA); donkey anti-rabbit IgG-Cy3 was used as the secondary antibody (#AP182C, 1:250; Santa Cruz Biotechnology, USA). The slides were mounted with Prolong™ Gold antifade reagent with DAPI mounting medium (Thermo Fisher Scientific, USA) and viewed under a confocal microscope equipped with Pascal 5 imaging software (Carl Zeiss, Germany). Terminal induction of BMSCs confirmed the ability of these cells to undertake trilineage differentiation into adipocytes, chondrocytes, and osteoblasts under published culture conditions (Cortes et al., 2013). A simple differentiation approach was applied using the StemPro® Adipogenesis, StemPro® Chondrogenesis, and StemPro® Osteogenesis differentiation kits (Life Technologies, CA, USA) according to the manufacturer's recommended protocols. Differentiation of BMSCs into adipocytes, chondrocytes, and osteoblasts was indicated by oil red O (Qian et al., 2010), alcian blue (Kazemnejad et al., 2012), and alizarin red S (Rickard et al., 1996) staining, respectively.

Differentiation of BMSCs into neural progenitor-like stem cells (NPCs)

BMSCs were induced into a neural lineage according to the protocol published previously (Huat et al., 2014). Briefly, BMSCs were dissociated with TrypLE™ Express and reseeded into ultra-low-attachment 96- or 6-well plates (depending on the assay) at a density of 1×10^5 cell/ml in neurobasal media containing the B-27™ Plus Neuronal Culture System, which is specific for rats (Thermo Fisher Scientific, USA). The cells were divided into three experimental groups: group A (neurobasal only), group B (10 ng/ml EGF +10 ng/ml bFGF), and group C (10 ng/ml EGF +10 ng/ml bFGF +10 ng/ml IGF-1). Growth factors, EGF (#GF155), bFGF (#GF003), and IGF-1 (#GF121), were purchased from Merck Millipore, USA. All groups were maintained at 37 °C with 5% CO_2 supplementation for 1 week, with fresh growth factors added every second day. Quantification of the size of each colony was conducted manually using ImageJ software. The cells were then subjected to cell proliferation and cell apoptosis assays.

On day 3 of neural induction, total RNA was extracted using the miRNeasy Mini Kit (Qiagen, Germany) according to the manufacturer's instructions and then reversed transcribed into cDNA using the High-Capacity RNA-to-cDNA Kit (Applied Biosystem, CA, USA). The newly synthesized cDNA was used as a template for detecting miR-22-3p and gene expression. Real-time PCR was conducted in a 20 μl reaction, using the TaqMan-based protocol on the StepOne™ Real-Time PCR system (Applied Biosystems, CA, USA). All reactions were run in triplicate using master mix and pre-designed primers as follows (all products were purchased from Applied Biosystem, CA, USA): for microRNA detection assay and endogenous controls: TaqMan Universal PCR Master Mix II, miR-22-3p (Assay ID: 000398), snoRNA (Assay ID: 001718), and small nucleolar RNA U87 (Assay ID: 001712); for gene expression assay and endogenous controls: TaqMan Fast Advanced Master Mix, *Akt-1* (Assay ID: Rn00583646_m1, RefSeq ID: NM_033230.2, Amplicon length: 87), *Tp53* (Assay ID: Rn00755717_m1, RefSeq ID: NM_030989.3, Amplicon length: 94), *Pten* (Assay ID: Rn00477208_m1, RefSeq ID: NM_031606.1, Amplicon length: 73), *Actb* (Assay ID: Rn00667869_m1, RefSeq ID: NM_031144.3, Amplicon length: 91), and *Gapdh* (Assay ID: Rn01775763_g1, RefSeq ID: NM_017008.4, Amplicon length: 174). Quantitative real-time PCR was performed at 95 °C for 10 min, followed by 40 cycles at 95 °C for 15 s and 60 °C for 1 min. Relative expression was calculated based on the $2^{(-\Delta\Delta Ct)}$ method using DataAssist™ software (Xia et al., 2010). Data were presented as fold change relative to the control.

Cell proliferation assay

To determine the proliferative potential of BMSC-derived NPCs, transfected BMSCs were resuspended into neural induction media and seeded into 96-well ultra-low-attachment plates (Corning, NY, USA) at a density of 1×10^4 cells/ml. Cellular proliferation was measured using the CellTiter 96® Aqueous One Solution Cell Proliferation Assay (Promega, WI, USA) according to the manufacturer's information. Briefly, the cells were incubated with the assay reagent for 4 h at 37 °C before the measurement of optical density (OD). The absorbance from each group was measured using a spectrophotometer at 24 h, 48 h, 72 h, 96 h, and 120 h post-induction at a wavelength of 490 nm using a spectrophotometer. Absorbance was recorded in triplicate from three independent experiments.

Cell survivability assay

The survival of BMSC-derived NPCs was assessed using apoptosis assay. This apoptosis assay was conducted with FITC-conjugated Annexin V and propidium iodide purchased from BD Biosciences Pharmingen, USA, according to the manufacturer's protocol. After treatment, apoptotic activities among groups were evaluated on days 1, 3, and 5 using quantitative data acquired from flow cytometric analysis. The experiment was performed in triplicate with three independent experiments.

MicroRNA transfection

BMSCs were seeded into a 6-well plate with the complete medium at a cell density of 2.5×10^5 cells/ml and incubated overnight. The following day, adherent cells were transfected with miR-22-3p inhibitor, miR-22-3p mimic, scramble hairpin inhibitor negative control #1, or scramble mimic negative control #1 (10 μM, Dharmacon, CO, USA) using the Lipofectamine® RNAimax transfection reagent (Life Technologies, USA), respectively. A different set of cells was concurrently transfected with a microRNA hairpin inhibitor conjugated with Dy547 (Dharmacon, CO, USA) to assess transfection efficiency. After 24 h of incubation, the cells were harvested for subsequence analysis. The transfection efficiency of BMSCs was determined with confocal microscopy (Carl Zeiss, Germany) and quantified using FACSCanto flow cytometry (BD Biosciences, CA, USA).

Dual-luciferase reporter assay

The sequence of three prime untranslated region (3′-UTR) of the wild-type *Akt1* was cloned downstream of the Gaussia luciferase (GLuc) secreted reporter gene and the secreted alkaline phosphatase (seAP) tracking gene (Genecopoeia, MD, USA). BMSCs were co-transfected with 15 pmol of either an miR-22-3p mimic or a scrambled mimic negative control #1 (C/N: IN-001005-01-05; Dharmacon, CO, USA) and 0.5 μg of a reporter plasmid using Lipofectamine 3000 as a transfection reagent (Life Technology, CA, USA) according to the manufacturer's protocol. GLuc and seAP activities were measured by luminescence in a conditioned medium 72 h after transfection using the Secreted-Pair Dual Luminescence Kit (Genecopoeia, MD, USA) following the manufacturer's protocol. Luminescence was measured using a Glomax 20/20 luminometer (Promega, WI, USA) with a 3 s integration time. Gaussian luciferase activity was normalized to alkaline phosphatase activity. Measurements were taken in quadruplicate from three independent experiments.

Transcriptomic library preparation

Total RNAs were extracted from 6 samples (BMSC samples at passage 3 from three SD rats (n = 3) and BMSC-derived NPC samples at day 3 derived under EGF + bFGF + IGF-1 supplementation (n = 3) using the MiRNeasy Mini Kit (Qiagen, Hilden, Germany) according to the manufacturer's protocol. The cDNA libraries were constructed as described previously (Khan et al., 2020). Briefly, 300 ng of total mRNA was enriched from each sample fragmented, followed by its conversion into cDNA. The cDNA was amplified using PCR. The created libraries were indexed, and then sequenced with the Nextseq®500 Sequencing System (Illumina, CA, USA) by setting a single-end sequence of 50 M reads per sample. All raw files were deposited openly in the GEO database NCBI with accession number GSE104548. The data files of the mRNA sequencing of the BMSC-derived NPCs derived with EGF and bFGF (Khan et al., 2020) were also used for the pairwise comparison with the BMSC-derived NPCs derived with IGF-1, EGF, and bFGF in this study.

Read pre-processing, QC, alignment, and gene quantification

Raw reads were evaluated for quality checks and then trimmed and filtered using BBDuk (BBMap - Bushnell B. - sourceforge.net/projects/bbmap/). The reads were then aligned to the latest reference genome (rn6) with GTF from Ensembl (v99) (Dobin et al., 2013) using the STAR aligner. Read counts were calculated per gene using the RSEM tool (Li and Dewey, 2011). The reads were normalized for depth and length, as described previously (Khan et al., 2020).

Differential expression analysis

Using the DESeq2 R package (Love et al., 2014), pairwise differential expression analysis was performed on NPCs derived with combinatorial EGF, bFGF, and IGF-1, with the transcriptome of the BMSCs serving as the reference. Selected differentially expressed genes were validated with the RT^2 Profiler PCR Array (Qiagen) (Table S1) according to the manufacturer's recommended protocol.

Gene ontology enrichment analysis and gene set enrichment analysis

In all comparisons, gene ontology enrichment analysis was performed on the differentially regulated genes using the Cytoscape v3.6.1 with the ClueGO v2.5.5 plugin (Shannon et al., 2003). The most significant GO terms were calculated, as described previously (Khan et al., 2020). Briefly, redundancy was reduced by grouping the GO terms according to their k-scores. Gene set enrichment analysis (FDR < 0.25) was also

performed, as described previously, against the gene sets from MSigDB (Subramanian et al., 2005).

3D terminal differentiation and electrophysiology recording

NPCs were seeded onto a semisolid collagen hydrogel matrix to mimic the 3D environment of the brain. Briefly, NPCs were first dissociated into a single-cell suspension using Accutase (Gibco) for 10 min. Dissociated cells were spun down and resuspended in NeuroCult® NS-A Differentiation media. Cells were seeded onto collagen hydrogel at 1.5×10^5 cells/well and cultured for 14 days in a humidified chamber at 37 °C with a 5% CO_2 supply. Half of the media was changed every two days, and the morphology of the cells was observed using an inverted light microscope.

Standard whole-cell patch clamp recording was performed on neuronal-like cells at 14 days, as described earlier (Khan et al., 2020). Neuronal-like cells cultured on a semisolid collagen hydrogel matrix were first superfused in ACSF at room temperature and continuously oxygenated throughout the recording. Microelectrode pipettes with an input resistance of 5–8 MΩ were fabricated from borosilicate glass capillary tubing using a P-97 micropipette puller. The perfusion bath was set to run at 1–2 ml per minute, and the gel slice was placed into the tub. The recording microelectrode pipette was then filled with an electrode solution. The microelectrode was placed in the pipette holder, and positive pressure was applied. The target cell was then slowly approached until changes in the test pulse amplitude were observed.

Cells with a neuronal-like morphology were chosen for the recording. Once a steady resistance was obtained, the positive pressure was released rapidly, and the resistance was allowed to gradually increase until a gigaohm (GΩ) seal was formed. Once the seal was formed, continuous light suction was applied until the membrane broke, as evidenced by a change in capacitance and test pulse current. Pulse protocols were generated, and current responses were recorded using a pClamp program interface. The recording was performed in triplicate, and a minimum of three cells from each group were recorded.

NPC transplantation

BMSCs at a density of 1×10^6 cells/ml were differentiated into NPCs in neural basal media supplemented with B-27™ Plus containing specific growth factors in an ultra-low-attachment 6-well plate. On day 3, NPCs were collected by centrifugation at 200 × g for 5 min. After gentle dissociation with the TrypLE™ Express stable trypsin replacement enzyme, the total cell number was adjusted back to 1×10^6 cells prior to pelleting at 200 ×g for 5 min. Cell pellets were then mixed with 5 μL of rat tail collagen I hydrogel (Gibco, Life Technologies, USA) and maintained on ice throughout the experiment. Neurospheres were transplanted one-off to the epicenter of the lesion site nine days after injury using a Hamilton syringe to the different groups (n = 3) as follow: sham group (no treatment), group 1 (hydrogel/vehicle), group 2 (hydrogel + NPCs derived from EGF + bFGF), and group 3 (hydrogel + NPCs derived from EGF + bFGF + IGF-1). Behavior analysis was performed to monitor the locomotor and sensory functions at 1 day post-transplantation and weekly after that.

The Basso, Beatie and Bresnahan (BBB) Scale and the Von Frey test

Locomotor function was measured using the BBB scale, a modified open-field test based on the hind limb locomotion, with a score range of 0 (no observable hind-limb movement) to 21 (normal activity) (Basso et al., 1995). After cell transplantation or control treatment, the BBB open-field locomotor rating scale was used weekly for 4 weeks. The experiment began with each rat being placed in the open field center, where uninjured or SCI rats could freely explore their environment for 5 min. Their movements were digitally recorded to assess the rats' hind limb locomotor frequency, joint movement range, and coordination (Qiu et al., 2015). The open-field floor was cleaned with 30% ethanol between trials and dried before the subsequent trial.

The sensory functionality of rat SCI was measured using the electronic Von Frey test (Deuis et al., 2017). All platform areas were sanitized with 70% ethanol solution before the test was carried out. Subjects were left undisturbed for a minimum of 30 min to acclimate to the wire grid and observation area. At the time of testing, all the rats were determined to be weight-bearing. Testing began with the left hind paw (paralysed hind limb). An increasing force (2–100 g) was applied using a von Frey filament to the plantar surface until the paw withdrawal threshold was reached (positive response). The filament is applied perpendicularly to the hindpaw. To ensure that sufficient force was applied and to distinguish true responses from the touch on responses, the filament hair was held for 3–5 s in place. Once the withdrawal threshold for the left rear foot was determined, the right hind paw (unaffected hind limb) was tested immediately after that. The test was repeated three consecutive times, between each of the fiber applications were allow 5 min interval on each paw to avoid artificial reduction in the withdrawal threshold and the paw withdrawal force results were recorded by the software post-test.

Hematoxylin and eosin (H&E) staining

The rats were sacrificed after the behavioral study was completed, 4 weeks post-transplantation. Spinal cords were carefully dissected and fixed in 10% neutral buffered formalin (Thermo Scientific, USA). The tissues were dehydrated overnight and embedded in paraffin wax. Transverse and longitudinal sections of the spinal cords with a thickness of 3 μm were stained with hematoxylin and eosin (H&E) and mounted with Cytoseal™ XYL (Thermo Scientific, USA). One normal thoracic section with no lesion evidence was identified and used as a reference for the cross-sectional area. An experienced pathologist viewed the images for histopathological analysis.

Gene expression using quantitative real-time PCR (qPCR)

The spinal cord tissues kept in the RNAlater™ solution were thawed and ground to fine tissue powder under liquid nitrogen. Total RNA was extracted using the innuPREP RNA Mini Kit 2.0 (Analytic Jena, Berlin, Germany) according to the manufacturers' instruction and stored at −80 °C. Reverse transcription of mRNAs was performed using the SensiFAST™ cDNA Synthesis Kit (Bioline, Meridian Bioscience Asia Pte Ltd, Singapore) using a Mastercycler Realplex thermal cycler (Eppendorf) with the following setup: primer annealing was at 25 °C for 10 min, reverse transcription at 42 °C for 15 min, inactivation at 85 °C for 5 min, and hold at 4 °C. Quantitative real-time PCR was performed using the SensiFAST™ Probe Hi-Rox Kit (Bioline, Meridian Bioscience Asia Pte Ltd, Singapore). The primer sequences were supplemented, as shown in Table S2. A similar annealing temperature (60 °C) was applied to all primer sequences. The polymerase activation was performed at 95 °C for 3 min, denaturation at 95 °C for 10 s, and annealing/extension at 60 °C for 30 s per kilobase pair for 40 cycles. The data were analyzed using the comparative C_T method, in which the relative foldchange ($2^{-(\Delta\Delta C)}_T$) of the respective gene expression between the treatment group (NPCs-transplanted) and the control group (untreated) was compared.

Western blot analysis

Spinal cord specimens were extracted with the T-PER™ Tissue Protein Extraction Reagent (Thermo Fisher Scientific, USA). Protein concentration was measured with the Pierce™ BCA Protein Assay Kit (Thermo Fisher Scientific, USA), according to the manufacturer's instructions. Total protein (10 μg/lane) was separated through sodium dodecyl sulfate-polyacrylamide gel electrophoresis (SDS-PAGE) and then transferred to activated polyvinylidene difluoride (PVDF) membranes using the iBlot2 dry blotting system (Thermo Fisher Scientific, USA). After that, the blotted membrane was immersed in 1 × iBind™ Solution (Thermo Fisher Scientific, USA). The membrane was then incubated with primary and secondary antibodies using the iBind™ Western System (Thermo Fisher Scientific, USA) at room temperature. The primary antibodies used included rabbit anti-Sox2 antibody, rabbit anti-nestin antibody, rabbit anti-beta III tubulin antibody, rabbit anti-Map2 antibody, rabbit anti-myelin basic protein antibody, GAPDH antibody (all 1:1000; Abcam, Cambridge, UK), rabbit anti-GFAP antibody (1:5000, Abcam, Cambridge, UK), and rabbit anti-APC antibody (1:50, Abcam, Cambridge, UK), followed by incubation with the secondary antibody, goat anti-rabbit IgG (HRP) (Thermo Fisher Scientific, USA). The signal was evaluated using the PierceTM ECL Western Blotting Substrate Kit (Thermo Fisher Scientific, USA). The protein band images were captured using a Fusion Fx

image analyzer (Vilber Lourmat, Germany) and quantified using ImageJ software.

Immunofluorescence and immunohistochemistry staining

For immunofluorescence staining, cells were fixed and incubated with mouse anti-CD90 FITC (1:100; Thermo Scientific, MA, USA), rat anti-CD44 PE (1:200; Abcam, Cambridge, UK), rabbit anti-CD11b PE (1:50, Abcam, Cambridge, UK), rabbit anti-fibronectin (1:100; Abcam, Cambridge, UK), rabbit anti-vimentin (1:100; Abcam, Cambridge, UK), mouse anti-Sox-2 clone 6G1.2 FITC (1:500; Merck Millipore, MA, USA), rabbit anti-beta III tubulin (1:1000; Abcam, Cambridge, UK), and rabbit anti-GFAP (1:100; Merck Millipore, MA, USA) overnight at 4 °C. Non-conjugated primary antibody was removed, and the cells were rinsed thrice in 1 × PBS for 5 min each. After washing, the cells were incubated with a secondary antibody for 2 h at room temperature. The secondary antibodies used were donkey anti-mouse IgG, Cy3 conjugated antibody (1:1000; EMD Millipore, MA, USA) and Donkey anti-rabbit IgG, Cy3 conjugated antibody (1:1000; EMD Millipore, MA, USA). Nuclei were counterstained with Sytox® blue nucleic acid stain (1:1000; Invitrogen, USA) for 10 min at room temperature and mounted with a fluorescence mounting medium. Samples were visualized using an LSM 5 Pa confocal microscope (Carl Zeiss, Germany). A negative control was carried out in which the primary antibody was omitted and replaced with buffer.

The paraffin-embedded tissues were sectioned transversally into 3 μm sections, processed for immunohistochemical staining, and later analyzed for histopathological changes. The primary antibodies included rabbit anti-Sox2 polyclonal (1:500; Abcam, Cambridge, UK) to label immature neurons, rabbit anti-nestin monoclonal (1:1000, Abcam, Cambridge, UK) to label neural progenitor cells (NPCs), rabbit anti-GFAP polyclonal (1:100; Abcam, Cambridge, UK) to label astrocytes, rabbit anti-APC monoclonal (1:50; Abcam, Cambridge, UK), and rabbit anti-MBP polyclonal (1:100, Abcam, Cambridge, UK) to label implanted MSCs using mouse and rabbit specific HRP/DAB IHC Detection Kit (Abcam, Cambridge, UK). All imaging was performed under the same exposure time and magnification for all stained slides. Images were then analyzed semi-quantitatively (Crowe and Yue, 2019). The DAB intensity was measured using ImageJ with the IHC toolbox plugin. The images were separated from H&E, and DAB brownish staining and the contrast/brightness level of brownish color were adjusted. The semi-quantitative measurement of DAB intensity was calculated in each image, and the results were expressed as optical density (OD).

Quantification and Statistical analysis

Statistical analyses

The data were analyzed using GraphPad Prism software version 9.0 (GraphPad Software, San Diego, CA, USA). All data are shown as mean ± SD, unless stated otherwise. Student's t-test was used to compare the mean difference between two groups, whereas one-way ANOVA was conducted to compare two groups and above. Differences with $p < 0.05$ were considered statistically significant.

References

Akcay, G., Luttge, R., 2021. Stiff-to-Soft transition from glass to 3D hydrogel substrates in neuronal cell culture. Micromachines 12, 165.

Alexanian, A.R., Maiman, D.J., Kurpad, S.N., Gennarelli, T.A., 2008. In vitro and in vivo characterization of neurally modified mesenchymal stem cells induced by epigenetic modifiers and neural stem cell environment. Stem Cell. Dev. 17, 1123–1130.

Alshawaf, A.J., Antonic, A., Skafidas, E., Ng, D.C.-H., Dottori, M., 2017. WDR62 regulates early neural and glial progenitor specification of human pluripotent stem cells. Stem Cell. Int. 2017, 7848932.

Ankrum, J.A., Ong, J.F., Karp, J.M., 2014. Mesenchymal stem cells: immune evasive, not immune privileged. Nat. Biotechnol. 32, 252–260.

Bai, X., Xiao, Z., Pan, Y., Hu, J., Pohl, J., Wen, J., Li, L., 2004. Cartilage-derived morphogenetic protein-1 promotes the differentiation of mesenchymal stem cells into chondrocytes. Biochem. Biophys. Res. Commun. 325, 453–460.

Basso, D.M., Beattie, M.S., Bresnahan, J.C., 1995. A sensitive and reliable locomotor rating scale for open field testing in rats. J. Neurotrauma 12, 1–21.

Benavides, F.P., Pinto, G.B.A., Heckler, M.C.T., Hurtado, D.M.R., Teixeira, L.R., Monobe, M.M.S., Machado, G.F., DE Melo, G.D., Rodríguez-Sánchez, D.N., Alvarenga, F., Amorim, R.M., 2021. Intrathecal transplantation of autologous and allogeneic bone marrow-derived mesenchymal stem cells in dogs. Cell Transpl. 30, 9636897211034464.

Berenguer, J., Herrera, A., Vuolo, L., Torroba, B., Llorens, F., Sumoy, L., Pons, S., 2013. MicroRNA 22 regulates cell cycle length in cerebellar granular neuron precursors. Mol. Cell Biol. 33, 2706–2717.

Chen, H., Lu, Q., Fei, X., Shen, L., Jiang, D., Dai, D., 2016. miR-22 inhibits the proliferation, motility, and invasion of human glioblastoma cells by directly targeting SIRT1. Tumor Biol. 37, 6761–6768.

Chouw, A., Facicilia, G., Pratiwi, E.D., Arofah, A.N., Sartika, C.R., Dirgantara, Y., Jundan, S.F., 2020. Basic fibroblast growth factor and epithelial growth factor could induce trans-differentiation of mesenchymal stem cell into neural stem cell. Cytotherapy 22, S75–S76.

Cohen, C.C.H., Popovic, M.A., Klooster, J., Weil, M.-T., Möbius, W., Nave, K.-A., Kole, M.H.P., 2020. Saltatory conduction along myelinated axons involves a periaxonal nanocircuit. Cell 180, 311–322 e15.

Cortes, Y., Ojeda, M., Araya, D., Dueñas, F., Fernández, M.S., Peralta, O.A., 2013. Isolation and multilineage differentiation of bone marrow mesenchymal stem cells from abattoir-derived bovine fetuses. BMC Vet. Res. 9, 133.

Crowe, A.R., Yue, W., 2019. Semi-quantitative determination of protein expression using Immunohistochemistry staining and analysis: an integrated protocol. Bio Protoc 9.

Deuis, J.R., Dvorakova, L.S., Vetter, I., 2017. Methods used to evaluate pain behaviors in rodents. Front. Mol. Neurosci. 10, 284.

Dobin, A., Davis, C.A., Schlesinger, F., Drenkow, J., Zaleski, C., Jha, S., Batut, P., Chaisson, M., Gingeras, T.R., 2013. STAR: ultrafast universal RNA-seq aligner. Bioinformatics 29, 15–21.

Dominici, M., LE Blanc, K., Mueller, I., Slaper-Cortenbach, I., Marini, F., Krause, D., Deans, R., Keating, A., Prockop, D., Horwitz, E., 2006. Minimal criteria for defining multipotent mesenchymal stromal cells. The International Society for Cellular Therapy position statement. Cytotherapy 8, 315–317.

Duncan, T., Valenzuela, M., 2017. Alzheimer's disease, dementia, and stem cell therapy. Stem Cell Res. Ther. 8, 111.

Fiumara, F., Rajasethupathy, P., Antonov, I., Kosmidis, S., Sossin, W.S., Kandel, E.R., 2015. MicroRNA-22 gates long-term heterosynaptic plasticity in Aplysia through presynaptic regulation of CPEB and downstream targets. Cell Rep 11, 1866–1875.

Hosseini, S.M., Sani, M., Haider, K.H., Dorvash, M., Ziaee, S.M., Karimi, A., Namavar, M.R., 2018. Concomitant use of mesenchymal stem cells and neural stem cells for treatment of spinal cord injury: a combo cell therapy approach. Neurosci. Lett. 668, 138–146.

Huang, Z.-P., Chen, J., Seok, H., Zhang, Z., Kataoka, M., Hu, X., Wang, D.-Z., 2013. MicroRNA-22 regulates cardiac hypertrophy and remodeling in response to stress. Circ. Res.

Huat, T., Khan, A., Abdullah, J., Idris, F., Jaafar, H., 2015a. MicroRNA expression profile of neural progenitor-like cells derived from rat bone marrow mesenchymal stem cells under the influence of IGF-1, bFGF and EGF. Int. J. Mol. Sci. 16, 9693–9718.

Huat, T.J., Khan, A.A., Abdullah, J.M., Idris, F.M., Jaafar, H., 2015b. MicroRNA expression profile of bone marrow mesenchymal stem cell-derived neural progenitor by microarray under the influence of EGF, bFGF and IGF-1. Genomics Data 5, 201–205.

Huat, T.J., Khan, A.A., Pati, S., Mustafa, Z., Abdullah, J.M., Jaafar, H., 2014. IGF-1 enhances cell proliferation and survival during early differentiation of mesenchymal stem cells to neural progenitor-like cells. BMC Neurosci 15, 91.

Jazbutyte, V., Fiedler, J., Kneitz, S., Galuppo, P., Just, A., Holzmann, A., Bauersachs, J., Thum, T., 2013. MicroRNA-22 increases senescence and activates cardiac fibroblasts in the aging heart. Age 35, 747–762.

Jin, Y., Tymen, S.D., Chen, D., Fang, Z.J., Zhao, Y., Dragas, D., Dai, Y., Marucha, P.T., Zhou, X., 2013. MicroRNA-99 family targets AKT/mTOR signaling pathway in dermal wound healing. PLoS One 8, e64434.

Karamouzian, S., Nematollahi-Mahani, S.N., Nakhaee, N., Eskandary, H., 2012. Clinical safety and primary efficacy of bone marrow mesenchymal cell transplantation in subacute spinal cord injured patients. Clin. Neurol. Neurosurg. 114, 935–939.

Kazemnejad, S., Akhondi, M.M., Soleimani, M., Zarnani, A.H., Khanmohammadi, M., Darzi, S., Alimoghadam, K., 2012. Characterization and chondrogenic differentiation of menstrual blood-derived stem cells on a nanofibrous scaffold. Int. J. Artif. Organs 35, 55–66.

Khan, A.A., Huat, T.J., AL Mutery, A., EL-Serafi, A.T., Kacem, H.H., Abdallah, S.H., Reza, M.F., Abdullah, J.M., Jaafar, H., 2020. Significant transcriptomic changes are associated with differentiation of bone marrow-derived mesenchymal stem cells into neural progenitor-like cells in the presence of bFGF and EGF. Cell Biosci. 10, 126.

Kim, D.Y., Hwang, I., Muller, F.L., Paik, J.H., 2015a. Functional regulation of FoxO1 in neural stem cell differentiation. Cell Death Differ. 22, 2034–2045.

Kim, S.J., Yu, S.-Y., Yoon, H.-J., Lee, S.Y., Youn, J.-P., Hwang, S.Y., 2015b. Epigenetic regulation of miR-22 in a BPA-exposed human hepatoma cell. BioChip J 9, 76–84.

Kim, Y.-C., Kim, Y.-H., Kim, J.-W., Ha, K.-Y., 2016. Transplantation of mesenchymal stem cells for acute spinal cord injury in rats: comparative study between intralesional injection and scaffold based transplantation. J. Kor. Med. Sci. 31, 1373–1382.

Kong, L.M., Liao, C.G., Zhang, Y., Xu, J., Li, Y., Huang, W., Zhang, Y., Bian, H., Chen, Z.N., 2014. A regulatory loop involving miR-22, Sp1, and c-Myc Modulates CD147 expression in breast cancer invasion and metastasis. Cancer Res 74.

Kuhn, S., Gritti, L., Crooks, D., Dombrowski, Y., 2019. Oligodendrocytes in development, myelin generation and beyond. Cells 8, 1424.

Laviola, L., Natalicchio, A., Giorgino, F., 2007. The IGF-I signaling pathway. Curr. Pharmaceut. Des. 13, 663–669.

Lee, J., Kuroda, S., Shichinohe, H., Ikeda, J., Seki, T., Hida, K., Tada, M., Sawada, K., Iwasaki, Y., 2003. Migration and differentiation of nuclear fluorescence-labeled bone marrow stromal cells after transplantation into cerebral infarct and spinal cord injury in mice. Neuropathology 23, 169–180.

Li, B., Dewey, C.N., 2011. RSEM: accurate transcript quantification from RNA-Seq data with or without a reference genome. BMC Bioinf. 12, 323.
Li, P., Fei, H., Wang, L., Xu, H., Zhang, H., Zheng, L., 2018. PDCD5 regulates cell proliferation, cell cycle progression and apoptosis. Oncol. Lett. 15, 1177–1183.
Littlejohn, E.L., Scott, D., Saatman, K.E., 2020. Insulin-like growth factor-1 overexpression increases long-term survival of posttrauma-born hippocampal neurons while inhibiting ectopic migration following traumatic brain injury. Acta Neuropathol. Comm. 8, 46.
Love, M.I., Huber, W., Anders, S., 2014. Moderated estimation of fold change and dispersion for RNA-seq data with DESeq2. Genome Biol. 15, 550.
Luo, L.-J., Zhang, L.-P., Duan, C.-Y., Wang, B., He, N.-N., Abulimiti, P., Lin, Y., 2017. The inhibition role of miR-22 in hepatocellular carcinoma cell migration and invasion via targeting CD147. Cancer Cell Int. 17, 17.
Mangiola, A., Vigo, V., Anile, C., DE Bonis, P., Marziali, G., Lofrese, G., 2015. Role and importance of IGF-1 in traumatic brain injuries. BioMed Res. Int. 12.
Medinaceli, L.D., 1986. An anatomical landmark for procedures on rat thoracic spinal cord. Exp. Neurol. 91, 404–408.
Meletis, K., Barnabé-Heider, F., Carlén, M., Evergren, E., Tomilin, N., Shupliakov, O., Frisén, J., 2008. Spinal cord injury reveals multilineage differentiation of ependymal cells. PLoS Biol 6, e182.
Mezey, E., Key, S., Vogelsang, G., Szalayova, I., Lange, G.D., Crain, B., 2003. Transplanted bone marrow generates new neurons in human brains. Proc. Natl. Acad. Sci. USA. 100, 1364–1369.
Mir, S., Cai, W., Carlson, S.W., Saatman, K.E., Andres, D.A., 2017. IGF-1 mediated neurogenesis involves a novel RIT1/akt/sox2 cascade. Sci. Rep. 7, 3283.
Mu, J., Li, L., Wu, J., Huang, T., Zhang, Y., Cao, J., Ma, T., Chen, J., Zhang, C., Zhang, X., Lu, T., Kong, X., Sun, J., Gao, J., 2022. Hypoxia-stimulated mesenchymal stem cell-derived exosomes loaded by adhesive hydrogel for effective angiogenic treatment of spinal cord injury. Biomater. Sci. 10, 1803–1811.
Mung, K.-L., Tsui, Y.-P., Tai, E.W.-Y., Chan, Y.-S., Shum, D.K.-Y., Shea, G.K.-H., 2016. Rapid and efficient generation of neural progenitors from adult bone marrow stromal cells by hypoxic preconditioning. Stem Cell Res. Ther. 7, 146.
Nieto-Estévez, V., Defterali, C., Vicario-Abejón, C., 2016. IGF-I: a key growth factor that regulates neurogenesis and synaptogenesis from embryonic to adult stages of the brain. Front. Neurosci. 10, 52.
Noguchi, S., Yasui, Y., Iwasaki, J., Kumazaki, M., Yamada, N., Naito, S., Akao, Y., 2013. Replacement treatment with microRNA-143 and -145 induces synergistic inhibition of the growth of human bladder cancer cells by regulating PI3K/Akt and MAPK signaling pathways. Cancer Lett 328, 353–361.
Okada, S., Nakamura, M., Katoh, H., Miyao, T., Shimazaki, T., Ishii, K., Yamane, J., Yoshimura, A., Iwamoto, Y., Toyama, Y., Okano, H., 2006. Conditional ablation of Stat3 or Socs3 discloses a dual role for reactive astrocytes after spinal cord injury. Nat. Med. 12, 829–834.
Pan, K., Deng, L., Chen, P., Peng, Q., Pan, J., Wu, Y., Wang, Y., 2019. Safety and feasibility of repeated intrathecal allogeneic bone marrow-derived mesenchymal stromal cells in patients with neurological diseases. Stem Cell. Int. 8421281.
Pang, S.H.M., D'Rozario, J., Mendonca, S., Bhuvan, T., Payne, N.L., Zheng, D., Hisana, A., Wallis, G., Barugahare, A., Powell, D., Rautela, J., Huntington, N.D., Dewson, G., Huang, D.C.S., Gray, D.H.D., Heng, T.S.P., 2021. Mesenchymal stromal cell apoptosis is required for their therapeutic function. Nat. Commun. 12, 6495.
Park, D., Xiang, A.P., Mao, F.F., Zhang, L., DI, C.G., Liu, X.M., Shao, Y., Ma, B.F., Lee, J.H., Ha, K.S., Walton, N., Lahn, B.T., 2010. Nestin is required for the proper self-renewal of neural stem cells. Stem Cell. 28, 2162–2171.
Qian, S.-W., Li, X., Zhang, Y.-Y., Huang, H.-Y., Liu, Y., Sun, X., Tang, Q.-Q., 2010. Characterization of adipocyte differentiation from human mesenchymal stem cells in bone marrow. BMC Dev. Biol. 10, 47.
Qiu, K., Huang, Z., Huang, Z., He, Z., You, S., 2016. miR-22 regulates cell invasion, migration and proliferation in vitro through inhibiting CD147 expression in tongue squamous cell carcinoma. Arch. Oral Biol. 66, 92–97.
Qiu, X.-C., Jin, H., Zhang, R.-Y., Ding, Y., Zeng, X., Lai, B.-Q., Ling, E.-A., Wu, J.-L., Zeng, Y.-S., 2015. Donor mesenchymal stem cell-derived neural-like cells transdifferentiate into myelin-forming cells and promote axon regeneration in rat spinal cord transection. Stem Cell Res. Ther. 6, 105.
Qu, J., Zhang, H., 2017. Roles of mesenchymal stem cells in spinal cord injury. Stem Cell. Int. 12.
Rickard, D.J., Kassem, M., Hefferan, T.E., Sarkar, G., Spelsberg, T.C., Riggs, B.L., 1996. Isolation and characterization of osteoblast precursor cells from human bone marrow. J. Bone Miner. Res. 11, 312–324.
Sandean, D., 2020. Management of acute spinal cord injury: a summary of the evidence pertaining to the acute management, operative and non-operative management. World J. Orthoped. 11, 573–583.
Satti, H.S., Waheed, A., Ahmed, P., Ahmed, K., Akram, Z., Aziz, T., Satti, T.M., Shahbaz, N., Khan, M.A., Malik, S.A., 2016. Autologous mesenchymal stromal cell transplantation for spinal cord injury: a Phase I pilot study. Cytotherapy 18, 518–522.
Serhan, A., Boddeke, E., Kooijman, R., 2019. Insulin-like growth factor-1 is neuroprotective in aged rats with ischemic stroke. Front. Aging Neurosci. 11.
Shannon, P., Markiel, A., Ozier, O., Baliga, N.S., Wang, J.T., Ramage, D., Amin, N., Schwikowski, B., Ideker, T., 2003. Cytoscape: a software environment for integrated models of biomolecular interaction networks. Genome Res 13, 2498–2504.
Shohayeb, B., Ho, U.Y., Hassan, H., Piper, M., Ng, D.C.H., 2020a. The spindle-associated microcephaly protein, WDR62, is required for neurogenesis and development of the Hippocampus. Front. Cell Dev. Biol. 8, 549353.
Shohayeb, B., Mitchell, N., Millard, S.S., Quinn, L.M., Ng, D.C.H., 2020b. Elevated levels of Drosophila Wdr62 promote glial cell growth and proliferation through AURKA signalling to AKT and MYC. Biochim. Biophys. Acta Mol. Cell Res. 1867, 118713.
Song, Y., Pimentel, C., Walters, K., Boller, L., Ghiasvand, S., Liu, J., Staley, K.J., Berdichevsky, Y., 2016. Neuroprotective levels of IGF-1 exacerbate epileptogenesis after brain injury. Sci. Rep. 6, 32095.
Su, Z., Niu, W., Liu, M.-L., Zou, Y., Zhang, C.-L., 2014. In vivo conversion of astrocytes to neurons in the injured adult spinal cord. Nat. Commun. 5, 3338.
Subramanian, A., Tamayo, P., Mootha, V.K., Mukherjee, S., Ebert, B.L., Gillette, M.A., Paulovich, A., Pomeroy, S.L., Golub, T.R., Lander, E.S., Mesirov, J.P., 2005. Gene set enrichment analysis: a knowledge-based approach for interpreting genome-wide expression profiles. Proc. Natl. Acad. Sci. USA 102, 15545.
Takeda, Y.S., Xu, Q., 2015. Neuronal differentiation of human mesenchymal stem cells using exosomes derived from differentiating neuronal cells. PLoS One 10, e0135111.
Tanna, T., Sachan, V., 2014. Mesenchymal stem cells: potential in treatment of neurodegenerative diseases. Curr. Stem Cell Res. Ther. 9, 513–521.
Tran, A.P., Silver, J., 2015. Systemically treating spinal cord injury. Science 348, 285–286.
Vaquero, J., Zurita, M., Rico, M.A., Bonilla, C., Aguayo, C., Fernández, C., Tapiador, N., Sevilla, M., Morejón, C., Montilla, J., Martínez, F., Marín, E., Bustamante, S., Vázquez, D., Carballido, J., Rodríguez, A., Martínez, P., García, C., Ovejero, M., Fernández, M.V., 2017. Repeated subarachnoid administrations of autologous mesenchymal stromal cells supported in autologous plasma improve quality of life in patients suffering incomplete spinal cord injury. Cytotherapy 19, 349–359.
Wang, H., Liao, S., Geng, R., Zheng, Y., Liao, R., Yan, F., Thrimawithana, T., Little, P.J., Feng, Z.-P., Lazarovici, P., Zheng, W., 2015. IGF-1 signaling via the PI3K/Akt pathway confers neuroprotection in human retinal pigment epithelial cells exposed to sodium nitroprusside insult. J. Mol. Neurosci. 55, 931–940.
Wang, T.Y., Park, C., Zhang, H., Rahimpour, S., Murphy, K.R., Goodwin, C.R., Karikari, I.O., Than, K.D., Shaffrey, C.I., Foster, N., Abd-EL-Barr, M.M., 2021. Management of acute traumatic spinal cord injury: a review of the literature. Frontiers in Surgery 8.
White, R.E., Jakeman, L.B., 2008. Don't fence me in: harnessing the beneficial roles of astrocytes for spinal cord repair. Restor. Neurol. Neurosci. 26, 197–214.
Wilkins, A., Majed, H., Layfield, R., Compston, A., Chandran, S., 2003. Oligodendrocytes promote neuronal survival and axonal length by distinct intracellular mechanisms: a novel role for oligodendrocyte-derived glial cell line-derived neurotrophic factor. J. Neurosci. 23, 4967–4974.
Wrigley, S., Arafa, D., Tropea, D., 2017. Insulin-like growth factor 1: at the crossroads of brain development and aging. Front. Cell. Neurosci. 11, 14.
Xia, M., Sherlock, J., Hegerich, P., You, X., Lee, K., Walworth, C., Spier, E., 2010. DataAssist™–Data analysis software for TaqMan® real-time PCR data. Proc. Int. MultiConf. Eng. Comp. Scientists 17–19.
Xiong, J., 2012. Emerging roles of microRNA-22 in human disease and normal physiology. Curr. Mol. Med. 12, 247–258.
Xiong, Y., Mahmood, A., Chopp, M., 2010. Angiogenesis, neurogenesis and brain recovery of function following injury. Curr. Opin. Invest. Drugs 11, 298.
Xu, D., Takeshita, F., Hino, Y., Fukunaga, S., Kudo, Y., Tamaki, A., Matsunaga, J., Takahashi, R.-U., Takata, T., Shimamoto, A., Ochiya, T., Tahara, H., 2011. miR-22 represses cancer progression by inducing cellular senescence. J. Cell Biol. 193, 409.
Xu, Q.-F., Pan, Y.-W., Li, L.-C., Zhou, Z., Huang, Q.-L., Pang, J.C.-S., Zhu, X.-P., Ren, Y., Yang, H., Ohgaki, H., Lv, S.-Q., 2014. MiR-22 is frequently downregulated in medulloblastomas and inhibits cell proliferation via the novel target PAPST1. Brain Pathol. 24, 568–583.
Yang, C., Ning, S., Li, Z., Qin, X., Xu, W., 2014. miR-22 is down-regulated in esophageal squamous cell carcinoma and inhibits cell migration and invasion. Cancer Cell Int. 14, 138.
Yi, C., Ma, C., Xie, Z., Zhang, G., Song, W., Zhou, X., Cao, Y., 2013. Down-regulation of programmed cell death 5 by insulin-like growth factor 1 in osteoarthritis chondrocytes. Int. Orthop. 37, 937–943.
Yu, M., Wang, H., Xu, Y., Yu, D., Li, D., Liu, X., DU, W., 2015. Insulin-like growth factor-1 (IGF-1) promotes myoblast proliferation and skeletal muscle growth of embryonic chickens via the PI3K/Akt signalling pathway. Cell Biol. Int. 39, 910–922.
Zhang, G.-M., Bao, C.-Y., Wan, F.-N., Cao, D.-L., Qin, X.-J., Zhang, H.-L., Zhu, Y., Dai, B., Shi, G.-H., Ye, D.-W., 2015. MicroRNA-302a suppresses tumor cell proliferation by inhibiting AKT in prostate cancer. PLoS One 10, e0124410.
Zhao, H., Wen, G., Huang, Y., Yu, X., Chen, Q., Afzal, T.A., Luong LE, A., Zhu, J., Ye, S., Zhang, L., Xiao, Q., 2015. MicroRNA-22 regulates smooth muscle cell differentiation from stem cells by targeting methyl CpG-binding protein 2. Arterioscler. Thromb. Vasc. Biol. 35, 918–929.
Zheng, Y., Xu, Z., 2014. MicroRNA-22 induces endothelial progenitor cell senescence by targeting AKT3. Cell. Physiol. Biochem. 34, 1547–1555.
Zuo, Q.F., Cao, L.Y., Yu, T., Gong, L., Wang, L.N., Zhao, Y.L., Xiao, B., Zou, Q.M., 2015. MicroRNA-22 inhibits tumor growth and metastasis in gastric cancer by directly targeting MMP14 and Snail. Cell Death Dis 6, e2000.